Contrasting diagenetic evolution patterns of platform margin limestones and dolostones in the Lower Triassic Feixianguan Formation, Sichuan Basin, China

LEI JIANG[a], RICHARD H. WORDEN[b], CHUNFANG CAI[a], ANJIANG SHEN[c], XUNYUE HE[c], LIYIN PAN[c]

[a]Key Laboratory of Petroleum Resources Research, Institute of Geology and Geophysics, Chinese Academy of Sciences, Beijing 100029, China

[b]Department of Earth, Ocean and Ecological Sciences, School of Environmental Sciences, University of Liverpool, Liverpool, L69 3GP, UK

[c]PetroChina Hangzhou Research Institute of Geology, Hangzhou 310023, China

ABSTRACT

Deeply-buried carbonate-reservoirs from the Lower Triassic Feixianguan Formation in the Sichuan Basin of China host extensive natural gas resources. These reservoirs are predominantly found in oolitic shoals, with the reservoir quality of dolomitized zones being higher than that of undolomitized limestone counterparts. Here we present a combination of petrographic, isotopic, fluid inclusion, and quantitative porosity data in order to understand and predict the diagenetic processes that have impacted the reservoir quality of dolostones and limestones. The porosity of limestones has been reduced to ~7.5% due to calcite cementation, whereas the porosity in oolitic dolostones is not cemented with calcite and typically has ~23.5% porosity. Dolomitization and concurrent early-diagenetic gypsum growth played crucial roles on the development and preservation of high porosity in the oolitic dolostone, first by stabilizing the rock fabric to inhibit loss of porosity during burial, and secondly through the generation of new porosity by dissolution of carbonate and anhydrite. A negative shift of $\delta^{18}O$ and salinity values (<3.5 wt. %) measured from fluid inclusions in diagenetic calcite cement in limestones suggest that diagenesis associated with meteoric water played a key role in destroying limestone reservoir quality. Early oil charge seems to have had a positive effect on carbonate reservoir quality in the dolostones, since oil emplacement inhibited calcite cementation. Subsequently, thermochemical sulfate reduction (TSR) occurred, predominantly in the dolostones, as shown by TSR calcite cement with highly negative $\delta^{13}C$ values (~ -20 ‰ VPDB) and $\delta^{18}O$ (~ -10 ‰ VPDB) together with elevated calcite precipitation temperatures (> 110°C). It is likely that TSR was responsible for the formation of enlarged dissolution vugs that increased porosity by ~2% in dolostones due to: i) anhydrite dissolution, ii) production of significant amounts of water resulting in formation water undersaturated with respect to calcite and dolomite, iii) generation of H_2S, and CO_2, and the consequent reaction of H_2S with the siderite ($FeCO_3$) component in calcite and dolomite. This study demonstrates the importance of diagenesis in the formation of deeply-buried, high-quality reservoirs in ooid-dominated grainstones influenced by the presence of evaporites. Our results should be useful for guiding future exploration and reservoir developments in similar paleogeographic and diagenetic settings.

Keywords: Feixianguan Formation, Sichuan Basin, carbonate reservoir, reservoir quality, diagenesis, dolomitization, thermochemical sulfate reduction, porosity evolution, fluid inclusion, C/O/Sr isotopes

1. Introduction

Porosity and permeability of carbonate successions generally decrease with burial depth (Schmoker and Halley, 1982; Lucia, 1995; Sun, 1995; Lucia, 2004; Ehrenberg et al., 2006). The reduction of porosity in limestones is caused predominantly by calcite cementation as a result of mechanical compaction, pressure-solution (chemical compaction)((Heydari, 2000). In contrast, deeply buried dolostone reservoirs normally show higher porosity compared to limestone because of reduced calcite cementation (Neilson and Oxtoby, 2008). The porosity of shallow-buried (< 3,500 m) dolostones (e.g., Pliocene-Pleistocene and Miocene dolostone) is typically equal to, or less than, the porosity in age-equivalent limestones (Lucia, 1995; Ehrenberg et al., 2006). However, there are some exceptional, shallow dolostone reservoirs that have higher porosity than their equivalent non-replaced limestones. Examples include the First Eocene reservoir at the giant Wafra Field (Saller et al., 2014), and the Miocene carbonate platforms of the Marion Plateau (Ehrenberg et al., 2006). As burial depth increases to more than 3,500 m, reservoir quality of dolostones tends to be better than that of limestone equivalents (Sun, 1995; Heydari, 1997; Ehrenberg et al., 2006; Jiang et al., 2014b; Jiang et al., 2016). This has been interpreted as a result of dolostones being more resistant to porosity-loss than limestones (i.e., more resistant to mechanical and chemical compaction and cementation) during progressive burial (Schmoker and Halley, 1982). Moreover, dolostone has been commonly reported to contain enlarged dissolution pores in deep burial environments (> 3,500 m) (Hugman III and Friedman, 1979). However, pores in deeply buried dolostone may have commonly been lined or plugged by late stage cements during deep burial diagenesis (Heydari, 1997; Loucks, 1999; Worden et al., 2000; Worden et al., 2004; Machel and Buschkuehle, 2008; Neilson and Oxtoby, 2008; Jiang et al., 2014a). ~~Diagenesis thus plays a significant role in the formation of reservoirs both in shallow and deeply buried carbonate successions.~~

The preservation of porosity in deeply buried dolostone reservoirs is predominately controlled by (i) the amount of remaining primary porosity (Choquette and Pray, 1970), (ii) the formation of secondary porosity due to replacement of calcite with dolomite (Sun, 1995; Machel, 2004a), although some authors have suggested that dolomite cementation could significantly reduce the reservoir quality (Lucia, 1995; Warren, 2000; Machel, 2004b), (iii) the dissolution of calcite or aragonite during dolomitization (Jiang et al., 2014b; Saller et al., 2014), as well as (iv) the preservation of the remaining early diagenetic porosity during burial (Choquette and Pray, 1970). Secondary pores generated by dissolution during deep burial diagenesis are unlikely to significantly contribute to reservoir quality, because pore fluids in sedimentary basins are typically saturated with carbonate and thus cannot dissolve carbonate minerals (Sun, 1995; Machel, 2004a; Ehrenberg et al., 2006; Ehrenberg et al., 2012; Dickson and Kenter, 2014). However, some case studies have reported that substantial porosity could be created during deep burial and/or uplift in carbonate reservoirs due to thermochemical sulfate reduction (TSR) (Ma et al., 2008a; Cai et al., 2014) and oxidation of the sulfate reduction-produced H_2S (Hill, 1995).

TSR is the abiological oxidation of hydrocarbons by sulfate at elevated temperatures (generally greater than 110 ºC), resulting in significant alteration of petroleum and the generation of a variety of reduced forms of sulfur (i.e., native S and H_2S) and oxidized forms of carbon (carbonate minerals and CO_2) as well as a combination of water, sulfide minerals, organosulfur compounds and bitumen (Machel, 1987; Machel et al., 1995; Worden et al., 1995; Worden et al., 2000; Bildstein et al., 2001; Cai et al., 2003; Jiang et al., 2015c).

A general reaction can be written as follows:

$$\text{sulfate} + \text{petroleum} \rightarrow \text{calcite} + H_2S \pm H_2O \pm CO_2 \pm S \pm \text{altered petroleum} \qquad \text{(R1)}$$

Recent studies have confirmed that TSR can generate substantial amounts of low salinity water (Worden et al., 1996; Jiang et al., 2015c). Consideration of the addition of this TSR water to deeply buried carbonate reservoirs may shed new light on mesogenetic secondary porosity generation and reservoir quality improvement (Worden et al., 1996; Jiang et al., 2015c).

Moreover, processes such as hydrothermal dolomitization, fluid mixing, fluid cooling, fracture system formation and brecciation, may also play important roles in causing mesogenetic dissolution in deep burial environments (Qing and Mountjoy, 1994; Sun, 1995; Machel, 2004a; Davies and Smith, 2006; Saller and Dickson, 2011; Hiemstra and Goldstein, 2015; Jiang et al., 2015b; Zhu et al., 2015).

The Lower Triassic Feixianguan Formation, present on the platform margin of the Kaijiang-Liangping Bay in the Sichuan Basin, offers a good opportunity to study the impact of both shallow and burial diagenesis on pore evolution (with depth of up to 7,500 m). Previous studies have shown that good quality reservoirs in this area are predominantly found in oolitic shoal facies present both at the platform margins and interiors, while dolomitized grainstones have much better reservoir quality compared to their limestone counterparts (Ma et al., 2008a; Jiang et al., 2014b; Chen et al., 2015; Wang et al., 2015; Qiao et al., 2016). Interparticle and dissolution-enhanced porosity (e.g., dissolution vugs, solution-enlarged pores or moldic pores) are the main pore types in these reservoirs (Ma et al., 2008a; Chen et al., 2015; Qiao et al., 2016). Most reservoirs in the northeast side (NE), and a few located in the southwest (SW) side, of the Kaijiang-Liangping Bay have been extensively dolomitized (Zhao et al., 2005; Jiang et al., 2014b). In contrast, most of the reservoirs in the SW side of Kaijiang-Liangping Bay are non-replaced limestones that have been heavily cemented by calcite and saddle dolomite (Cai et al., 2014; Jiang et al., 2014b; Zhou et al., 2014). This paper focuses on documenting and understanding the different diagenetic processes that have affected oolitic limestone and oolitic dolostone reservoirs from platform margin shoal and platform interior shoal facies in the Feixianguan Formation. We aim to determine the effects of dolomitization and TSR on the rock properties in deeply buried carbonate gas reservoirs. Specifically, this study seeks to address the following research questions:

1. What diagenetic processes have occurred and how have they affected pore evolution in coeval lime- and dolo-grainstone reservoirs?

2. What are the factors that have controlled the presence of good reservoir quality in the deeply buried Feixianguan Formation?

3. Can TSR improve reservoir quality, and if so, by what mechanisms?

2. Geological setting

The intracratonic Sichuan Basin is located in the east of the Sichuan Province, southwest China and has an area of about 230,000 km^2 (Fig. 1A). The Sichuan Basin is tectonically-bounded by the Longmenshan fold belt to the northwest, the Micangshan uplift in the north, the Dabashan fold belt the northeast, the Hubei-Hunan-Guizhou fold belt to the southeast, and by the Emeishan-Liangshan fold belt to the southwest.

The Lower Triassic Feixianguan Formation was deposited in a tidal-dominated, platform margin, oolitic shoal complex. It belongs to the highstand system tract (HST) of a single composite sequence and comprises several shallowing upward sequences consisting, from base to top, of grain-dominated packstone, cross- bedded ooid grainstone, laminated dolomudstone with fenestral porosity, and multiple gypsiferous layers, due to fluctuating sea-level and the predominantly arid climate of the time (Fig. 1B) (Zhao et al., 2005; Qiao et al., 2016). These gypsum beds, together with the anhydrite and halite in the overlying Jialingjiang Formation, comprise the regional seal for the underlying carbonate reservoirs (Fig. 2) (Zhao et al., 2005). A semi-isolated evaporitic carbonate platform formed on the northeast (NE) side of Kaijiang-Liangping Bay, whereas an open carbonate platform developed on the southwest (SW) side (Zhao et al., 2005; Ma et al., 2008a). Hence, the Feixianguan Formation on the NE side of Kaijiang-Liangping Bay is more rich in dolomite than the SW side, probably due to a locally more restricted environment in the NE side (Zhao et al., 2005; Jiang et al., 2014b).

The Feixianguan Formation reached its maximum burial of 7,500 m, and temperatures of 220°C, due to initial progressive burial; after this it was followed by variable uplift (Fig. 3), resulting in Triassic reservoir temperatures between 100 and 140°C and depths between 3,000 and 6,000 m at the present day (Ma et al., 2008a). Gases in the Feixianguan Formation reservoirs have variable H_2S concentrations, predominantly between 10 % and 20 % (Cai et al., 2004; Li et al., 2005; Hao et al., 2008; Cai et al., 2010; Liu et al., 2013; Liu et al., 2014; Hao et al., 2015) with H_2S $\delta^{34}S$ values being close to the parent anhydrite $\delta^{34}S$ values (Zhu et al., 2005; Cai et al., 2010).

Reservoir quality of limestone and dolostone reservoirs in the research area shows great heterogeneity, which overall has been strongly influenced by sedimentary facies with significant diagenetic creation of secondary porosity and vertical flow barriers (e.g. lithofacies barriers, pore-type-change barriers, and cemented-zone barriers) that separated the reservoir into flow units (Zhao et al., 2005; Ma et al., 2008b; Qiao et al., 2016). The best reservoirs, with thicknesses up to 300 m at depths > 5,000 m, are primarily found in the oolitic shoal facies deposited in a high-energy, shallow-water environment (Ma et al., 2008b). Porosity (0-30 %) and permeability (0.01-10,000 mD) in oolitic dolostone reservoirs present in the upper part of HST are significantly higher than their oolitic limestone counterparts, which are typically present in the middle part of the same HST (Fig. 2).

3. Methodology

218 core samples from 23 wells, containing various diagenetic phases and carbonate host rocks (e.g. limestone, dolostone), were collected from cores of the Lower Triassic Feixianguan Formation from the Puguang, Maoba, Luojiazhai, Dukouhe, Longgang, Tieshan, and Yuanba sour gas fields (Fig. 1A). 168 thin sections (30 µm thick) were stained with Alizarin Red S to differentiate calcite and dolomite and their ferroan versions (Dickson, 1966). Selected polished thin samples were examined by scanning electron microscope (SEM) in backscattered electron imaging mode (BSEM). Point counting was used to determine the mineral composition and pore type. 72 grainstone, 28 limestone and 44 dolostone samples were selected for point counting to quantify the various carbonate cement and diagenetic mineral and grain populations (Table 1).

Fluid inclusion homogenization temperatures (Th) were measured from fluid inclusion assemblages (FIAs) containing two-phase aqueous inclusions in five doubly-polished (50 to 60 µm thick) wafers. The use of FIAs to determine temperatures of mineral growth, as opposed to single inclusions, gives confidence that the Th data are credible and minimises the effects of artefacts, such as thermal re-equilibration (Goldstein & Reynolds (1994) and Goldstein (2012).

Fine powder samples were extracted from cores using low-speed micro-drill and used for strontium, carbon, and oxygen isotopic measurements. Approximately 60 mg of powder from 15 samples were extracted for strontium isotope analysis. Calcite and dolomite samples were leached in 0.5 molar acetic acid at room temperature for 4 hours and 3.4 molar acetic acid at 60°C for 24 hours, respectively. The strontium in each component was further separated by conventional cation exchange techniques using ion exchange resin (packed with Bio-Rad AG50Wx8). Strontium isotope analyses were performed on a Finnigan MAT-262 multi-collector thermal ionization mass spectrometer (TIMS). The measured values for the NBS-987 standard were $^{87}Sr/^{86}Sr$: 0.710256 ±0.000014 (n = 8, 1 SD). Over the course of the analyses, the Sr blank was lower than 300 pg.

Approximately 30-50 mg samples of ten vug/fracture filling calcite samples, collected from limestone dominated reservoirs, were extracted for $\delta^{13}C$ and $\delta^{18}O$. Calcite powered samples were then reacted with anhydrous phosphoric acid, under vacuum, to release CO_2 at 25°C for 24h. The CO_2 was then analyzed for carbon and oxygen isotopes on a Finnigan MAT251 mass spectrometer standardized with NBS-18. All $\delta^{13}C$ and $\delta^{18}O$ are reported in ‰ units relative to the Vienna Peedee Belemnite (VPDB) standard. The precision for both $\delta^{13}C$ and $\delta^{18}O$ measurements is better than ±0.1‰.

4. Results

4.1. Petrography and paragenetic sequence

The entire paragenetic sequence in the studied Feixianguan Formation consists of 23 distinct events. The relative timing of these phases is based on superposition and cross-cutting of various features, as well as homogenization temperatures derived from various diagenetic minerals (see details below). It should be noted that information about limestone represent new data generated during this study, which has here been compared to the paragenetic sequence in dolostone by summarising and referring to previous studies (Li et al., 2012; Cai et al., 2014; Jiang et al., 2014a; Jiang et al., 2015a).

Micrite envelopes represent the first diagenetic phase; they are typically 10 to 50 μm wide, and surround ooids (Fig. 4A, B). Extensive micritization led to the total destruction of the carbonate grain fabric. Calcite-1 cement (Phase 2) followed, or was synchronous with, micrite envelopes. Calcite-1 occurs as isopachous rims, fine-crystalline (<50 μm) equant fringes to ooids (Fig. 4A), or infills to fenestral pores. Calcite-1 locally led to a reduction of primary porosity. Dolomite-1 is microcrystalline (Fig. 6A) and is spatially associated with restricted lagoon facies; it is more abundant in the NE than SW side of Kaijiang-Liangping Bay. Ooids were either partially or totally dissolved (dissolution-1, also Phase 3) during the initial dolomitization process in dolostone reservoirs (Fig. 7A, B) in the NE side of Kaijiang-Liangping Bay; oomoldic pores are commonly found in the upper part of shallowing upward sequences (Zhao et al., 2005). Diagenetic sulfate minerals, (e.g., sedimentary bedded anhydrite, isolated anhydrite nodules, anhydrite and celestite cements (Phase 4), have been found in the Fiexianguan Formation in the NE side of Kaijiang-Liangping Bay (Fig. 8A). There are signs of a dissolution event (dissolution-2, Phase 5) both in limestone and dolostone samples in which some ooid grains are partially or totally dissolved (Figs. 2B, 4A, 6A, B); some oomoldic pores were found in the top of shallowing upward sequences in the SW side of Kaijiang-Liangping Bay. Calcite-2 cement (Phase 6) occurs as fibrous to bladed crystals that have grown on top of calcite-1 or filled early moldic pores (Fig. 4B) in limestone (Dissolution 1) on the SW side of Kaijiang-Liangping Bay. Dolomite-2 (Phase 7) represents the second dolomitization event in the Feixianguan Formation. This dolomite type was the result of the reflux of mesohaline water and/or caused by seawater dolomitization at relatively low temperatures (~35 to 40 ºC) during early burial diagenesis (Fig. 6A) in both sides of the Kaijiang-Liangping Bay (Jiang et al., 2014b).

Pressure solution features and calcite-3 cementation are common in Feixianguan limestone (Phase 8) (Fig. 4C), but rarely observed in Feixianguan dolostone (Fig. 5A). The most obvious evidence for pressure solution is stylolites (pressure-solution seams) (Koehn et al., 2016), which form fitted fabrics, and occur as narrow, undulating, dark grey to black seams. Calcite in limestone reservoir occurs as very coarsely crystalline (up to several centimetres in size) pore-filling calcite cement in limestone reservoirs (Fig. 4B).

An early episode of exotic mineral growth (Phase 9) is characterised by mineralization with localised trace quantities of barite, fluorite, quartz and celestite (Fig. 8B, D) in the NE side of Kaijiang-Liangping Bay (Jiang et al., 2014a). Mineralization is unlikely to have had a regionally significant effect on Feixianguan Formation reservoir quality.

Fracture-1 (Phase 10) probably developed during, or after, Phases 6-9, both in limestone and dolostone, based on the crosscutting relationships to stylolites and late fractures. The fractures are variable in size and intensity (in terms of fractures per cm); they are commonly vertical to subvertical, with apertures range from centimetres to meters (Fig. 9A).

Phases 11 to 19 are mostly found in dolostones in NE side of Kaijiang-Liangping Bay. Dolomite-3 represents the third dolomitization event in the Feixianguan Formation (Phase 11). It occurs as coarsely crystalline, fabric destructive dolomite and/or dolomite cement (Fig. 6B). Based on detailed fluid inclusion and $^{87}Sr/^{86}Sr$ data, dolomite-3 formed at a temperature range between 80 and 140ºC, by the invasion of brine derived from the slightly younger, but also early Triassic, Jialingjiang Formation (Jiang et al., 2014b).

Oil charging (Phase 12) occurred during progressive burial when reservoir temperatures reached 80ºC (Ma et al., 2008a), with the oil supplied from the underlying, slightly hotter, Permian source rocks (Hao et al., 2008; Cai et al., 2010). It is evident that dolostone reservoirs contain variable amounts of solid bitumen, and, in some intervals, the bitumen content is abnormally high (Hao et al., 2008). Solid bitumen occurs as a pervasive “stain” in interparticle and intercrystal pore spaces, coatings or “blobs” in secondary pore spaces (Figs. 5B; Fig. 7A, C), as well as cement in fractures and bitumen-bearing fluid inclusions in calcite cements. Dissolution-3 (Phase 13) happened during the oil charge stage, possibly associated with organic or carbonic acid released from the source rocks (Hao et al., 2008; Ma et al., 2008a; Cai et al., 2014).

Calcite-4 (Phase 14) is present as coarsely crystalline, pore-filling and fracture-filling cements, mostly in dolostone reservoirs. Oil/bitumen, and gas fluid inclusions are locally present both the edges and throughout calcite-4 (Fig. 5B, C) suggesting that it grew during late diagenesis, most likely after petroleum charging. Native (elemental) sulfur (Phase 15) occurs as subhedral, coarse-crystalline accumulations in some samples, as crenulated blobs, and as a fine-crystalline coating in fractures and secondary voids. Native sulfur is intergrown with bitumen, pyrite, and calcite-4. Locally pyrite (Phase 16) occurs as millimetre- size cubic crystals, although it is also found as framboidal aggregates with single micrometer- size crystals. Most millimetre- size pyrite occurs as traces in dolostone reservoirs (Fig. 8C), and commonly is the last cement after dolomite-3 and calcite-4; pyrite shows a close growth relationship with native sulfur (Phase 15). Dissolution-4 (Phase 17) created some enlarged pores that are partly filled with bitumen, calcite-4, native sulfur, and pyrite (Fig. 7C, D) (Jiang et al., 2014a). Fracture-2 (Phase 18) occurs at variable sizes and intensities (number per cm), and is commonly vertical to sub-vertical, with sizes range from centimetres to meters (Fig. 9A). Fracture-2 locally crosscuts fracture-1 and is commonly filled by calcite, indicating it was formed after fracture-1. Gas charged the dolostone reservoir (Phase 19) due to increasing temperature during progressive depth of burial of the Feixianguan Formation and the underlying Permian source rock. In this temperature realm (~100 to 200ºC), oil progressively transforms into gas, and TSR has been shown to promote oil cracking in the Feixianguan Formation (Hao et al., 2008; Ma et al., 2008b).

A third phase of fracturing (fracture-3, Phase 20) cutting all the other minerals occurs both in limestone and dolostone reservoirs and occurred after TSR-related events 14-19 (Guo, 2010; Jiang et al., 2014a). The fractures occur at variable sizes and densities, and are commonly vertical to sub-vertical, with sizes range from centimetres to meters. Fracture-3 features are locally filled by the slightly later calcite-5 (Phase 21, Fig. 5D) in dolostone and late diagenetic calcite-3 in limestone, but some fractures are open without any infillings (Fig. 9B). A fifth phase of dissolution (dissolution-5, Phase 22) created localised void spaces. In some dolostone intervals in the NE side of Kaijiang-Liangping Bay. Phase 23 in the diagenetic sequence is represented by localized fracture-filling celestite, anhydrite, and barite in the dolostone reservoirs in the NE side of Kaijiang-Liangping Bay. Celestite, anhydrite, and barite are locally present in the dolostone reservoir in very small volumes, and occur as late diagenetic, coarsely crystalline minerals that contain two phase aqueous fluids inclusions (Jiang et al., 2014a).

4.2. Mineralogy of limestone and dolostone

Point counted mineral proportions from 72 oolitic dolostone and limestone samples from the Feixianguan Formation platform margin shoal facies and platform interior shoal facies are listed in Table 1. The most common components include: dolomite, calcite, bitumen, diagenetic pyrite and quartz. Limestone is predominantly composed of ooids, matrix, and early calcite cements (calcite-1, calcite-2, and calcite-3), with total solid mineral (grain and cement) volumes of more than 90 % (Fig. 10). Late diagenetic calcite (calcite-4) and pyrite are effectively absent (~ 0%) in limestone samples. Average volumetric percentages of early calcite cement in oolitic limestone are as follows (Fig 10. A, B): (1) calcite-1: 11.1 ± 10.4% (n=14) in the platform interior shoal and 5.9 ± 2.2% (n=14) in the platform margin shoal; (2) calcite-2: 15.3 ± 10.4% (n=14) in the platform interior shoal and 15.2 ± 12.9% (n=14) in the platform margin shoal; (3) calcite-3: 28.3 ± 10.4% (n=14) in the platform interior shoal and 13.2 ± 12.6% (n=14) in the platform margin shoal. Other diagenetic minerals, such as dolomite, quartz and bitumen, are locally present in small volumes (with a total volume <5 %) in limestone (Table 1, Fig. 11).

Oolitic dolostone consists of dolomitized ooids and dolomite cements (dolomite-1, dolomite-2, and dolomite-3), with average values of 84.2% in the platform interior shoal and 82% in the platform margin shoal (Fig. 10C, D). In contrast to limestone, dolostone samples have negligible calcite-1, calcite-2, and calcite-3, contain lower amounts of calcite-4, but also contain some pyrite (Phase 16). Average volumetric percentages of carbonate cements and bitumen are as follows (Fig. 10C, D): (1) calcite-1 and calcite-2: 0 % both in the platform interior shoal and platform margin shoal; (2) calcite-3: 0% in the platform interior shoal and 0.6 ± 3.1 % (n=29); (3) calcite-4: 1.5 ± 1.8 % (n=15) in the platform interior shoal and 1.7 ± 4.0 % (n=29) in the platform margin shoal; (4) dolomite-1, 2: 9.9 ± 7.6 % (n=15) in the platform interior shoal and 7.9 ± 7.2 % (n=29) in the platform margin shoal, dolomite-3: 8.1 ± 6.8 % (n=15) in the platform interior shoal and 5.6 ± 7.0 % (n=29) in the platform margin shoal; (5) bitumen: 3.6 ± 3.1 % (n=15) in the platform interior shoal and 4.8 ± 6.2 % (n=29) in the platform margin shoal. Other diagenetic minerals in dolostone reservoirs (quartz, and calcite-5) collectively have a minor total volume of less than 0.5 %.

4.3. Porosity and pore systems

Porosity in lime-grainstone is relatively low, ranging from 0 to 10 %, with most values less than 5 % (Table 1). The average porosity value of 1.9 % ± 2.4 (n=14) in the platform interior shoal and 2.2 ± 3.4% (n=14) in the platform margin shoal (Table 1), is similar to the reported core analysis porosity data from the study area (Fig. 2B) (Cai et al., 2014; Wang et al., 2015; Qiao et al., 2016). Dolo-grainstones commonly have higher porosity values between 0 to 33 %, with an average of 9.1 ± 4.9 % (n=15) in the platform interior shoal and 10 ± 8.5 % (n=29) in the platform margin shoal (Table 1; Fig. 10C, D). These values are also similar to available core analysis porosity data (Fig. 2C) (Zhao et al., 2005; Ma et al., 2008a; Cai et al., 2014; Chen et al., 2015; Wang et al., 2015; Qiao et al., 2016).

Pore type classification in this study follows Choquette and Pray (1970). The reservoirs contain pore types that are highly variable and include both primary and secondary pores. These pores are listed in order of importance as follows: solution-enlarged pores, oomoldic, interparticle, intercrystalline, and fracture (Fig 4A; Fig. 7).

4.3.1. Solution-enlarged pores/vugs

Pores/vugs in dolostone reservoirs are dominated by solution-enlarged pores (Fig. 7). This pore type has two main occurrences. The first is characterised by solution-enlarged pores and vugs where some ooids have been completely dissolved leading to large sized (up to 2 mm) dissolution pores (Figs. 7C). The second type is characterised by partial or complete dissolution of dolomite crystals (Figs. 7D). Dissolution-enlarged pores are locally filled by calcite-4, pyrite, native sulfur, and bitumen. Dolostone reservoirs with dissolution enlarged pores/vugs have the highest porosity and permeability in the Feixianguan Formation (Zhao et al., 2005; Cai et al., 2014; Hao et al., 2015).

4.3.2. Oomoldic pores

Grain-supported fabrics are common in the Feixianguan Formation. Ooids are the dominant grain type, with peloids and bioclasts locally present in minor quantities. In dolostone reservoirs, fabric destructive dolomite mainly consists of "ooid ghosts" and has some dolomite cements within interparticle pores. Some ooids are partially dissolved, but locally filled with late diagenetic minerals (e.g. calcite, dolomite, anhydrite, and quartz) both in limestone and dolostone reservoirs (Fig. 4A; Figs. 7A, B) (Guo, 2010). Some ooids have been completely dissolved, resulting in the formation of open moldic porosity.

4.3.3. Interparticle pores

Interparticle pores in dolostone reservoirs are commonly observed throughout the Feixianguan Formation (e.g., Fig. 6A). This pore type is commonly associated with solution-enlarged pores and it is not possible to determine their total volume. Although widespread, this is not the dominant pore type and does not significantly contribute to the present day overall porosity.

4.3.4. Intercrystalline pores

The most porous dolostones have intercrystalline porosity (Figs. 6B and 7D). The most representative one is dolomudstone in lagoon facies rocks (Zhao et al., 2005). Some of intercrystalline pores are filled with early or late diagenetic anhydrite and/or celestite cements in areas near, or within, the lagoonal facies. Intercrystalline pores were not subjected to these early and late cements in areas near to, or within, the platform margin shoal facies (Jiang et al., 2014b).

4.3.5. Fracture porosity

Some open fractures are locally present both in limestone and dolostone reservoirs (Guo, 2010), and these fractures cross-cut all the other diagenetic minerals (Fig. 9B). This suggests that fracture-3 pores formed during the latest uplift stage. However, fracture porosity does not contribute much porosity to the Feixianguan Formation because fractures are highly localized distribution and many are filled by calcite-5 (Guo, 2010; Jiang et al., 2014a).

4.4. Geochemical results

4.4.4. Aqueous inclusion homogenization temperature and salinity

Diagenetic carbonate minerals, such as fracture-filling, non-TSR calcite (calcite-3 and calcite-5), pore-filling TSR calcite (calcite-4), and deep burial dolomite (dolomite-3), all contain primary, two-phase aqueous inclusions filled with fluids that may reflect the trapping conditions (Goldstein and Reynolds, 1994b). We have previously reported fluid inclusion data in these late diagenetic carbonate and non-carbonate minerals in the Feixianguan dolostone reservoirs (Jiang et al., 2014a; Jiang et al., 2014b; Jiang et al., 2015c). In this study, we have produced new fluid inclusion data from calcite-4 samples (the dominant calcite cement) and calcite-5 (minor calcite cement) from limestone host rocks. Our new data show that calcite-4 in limestone has homogenization temperatures ranging from about 70ºC to 120ºC with a modal value of about 90ºC; calcite-5 in limestone has homogenization temperatures mainly ranging from 130ºC to 170ºC (Figs. 11A, E, Fig. 12A). The calcite-3 samples have relatively low salinities ranging from 0.35 % wt NaCl to 3.7 % wt NaCl, whereas calcite-4 samples have relatively high salinities of about 10 % wt NaCl (Figs. 11B, F, Fig. 12B). Homogenization temperature and salinity data of calcite-3 and calcite-5 in the dolostone reservoirs can be compared to the calcite-3 and calcite-5 data from limestone host rocks (Figs. 11C, D, E, F).

4.4.2. Stable carbon and oxygen isotopic analyses

In detail, new isotopic data show that calcite-2 has $\delta^{13}C$ values from -2.5 to 2.8 ‰ V-PDB. However, calcite-2 $\delta^{13}C$ values predominantly lie between 1.5 and 2.5 ‰ V-PDB, being close to the $\delta^{13}C$ values of bulk dolostones

(Jiang et al., 2014b), bulk limestones (Jiang et al., 2015a) and calcite-5 (Jiang et al., 2014a) (Table 2; Figs. 13a, b). In contrast, calcite-4 in dolostones, has a broadly negative spread of $\delta^{13}C$ values, ranging from -18.9 ‰ up to about 1.5‰ V-PDB (Fig. 13b). Calcite-2 has $\delta^{18}O$ values from -7.2 to -3.8‰ V-PDB (Table 2; Fig. 13a). Bulk limestone samples have $\delta^{18}O$ values between -6.0 to -4.5‰ V-PDB (Fig. 13a).

4.4.3. Radioactive strontium isotopic analyses

Bulk limestone samples and calcite-2 samples in limestone show relatively low $^{87}Sr/^{86}Sr$ ratios, ranging from 0.70720 to 0.70750, and 0.7073 to 0.70765, respectively (Fig. A). Both are well within the published range of coeval Feixianguan seawater $^{87}Sr/^{86}Sr$ values (Fig. 14) (Jiang et al., 2014b). Calcite-4 and calcite-5 have $^{87}Sr/^{86}Sr$ ratio ranges that overlap with bulk limestone and calcite-2, with values lying between 0.70720 and 0.70765 (Fig. 14B) (Jiang et al., 2015a). Dolomite-1, dolomite-2, and dolomite-3 show relatively wider and slightly higher ranges of $^{87}Sr/^{86}Sr$ ratios from 0.70730 to 0.70800 (Jiang et al., 2013; Jiang et al., 2014b).

5. DISCUSSION AND INTERPRETATION

5.1. Interpretation of diagenetic history

The paragenetic sequences for the two lithologies, limestone and dolostone, both show similarities and differences to those reported from earlier studies of Lower Triassic carbonates in the Sichuan Basin (Cai et al., 2004; Hao et al., 2008; Cai et al., 2014; Jiang et al., 2014a; Hao et al., 2015; Jiang et al., 2015c). Three overall stages have previously been defined (Jiang et al., 2014a) that represent the diagenetic history in the Feixianguan Formation (Fig. 15): (i) pre-TSR diagenesis, Phases 1 to 13, (ii) TSR diagenesis, Phase 14-19, and (iii) post-TSR diagenesis, Phase 20-23. These three diagenetic stages have been constrained by a combination of: temperature of cementation, cement composition, or sources of the diagenetic fluids inferred from geochemical data.

Pre-TSR diagenetic processes commenced with the development of micrite envelopes and calcite-1 cementation, in the marine environment, both in limestones and dolostones. The subsequent diagenetic processes in limestone were significantly different to those in dolostone. In dolostone, the pre-TSR diagenetic stage included two stages of dolomite growth. The dominant initial dolomitization (dolomite-1 and dolomite-2) commenced at relatively low temperatures, from 35 to 40 ºC as shown by (Jiang et al., 2013), under near-surface conditions or at very shallow burial (< 500 m) (Jiang et al., 2014b). Burial dolomite (dolomite-3) developed at intermediate burial environments with temperatures ranging between 80 and 140ºC (Jiang et al., 2014b). The increasing $^{87}Sr/^{86}Sr$ ratios in these dolostones (Fig. 15) suggest that some dolomitization fluids may have been influenced by an influx of younger Jialingjiang brines (Jiang et al., 2014b). Anhydrite cement growth accompanied the main early reflux dolomitization stage (dolomite-1 and dolomite-2). In contrast, there is a lack of anhydrite cementation in limestone. Significant calcite cementation (calcite-3) occurred predominantly in limestone and resulted in almost complete loss of porosity. Oil subsequently charged the dolostone reservoirs during progressive burial but the limestones were not charged since they had negligible remaining porosity (and thus vanishingly low permeability).

Thermochemical sulfate reduction (TSR) diagenesis most commonly occurred in dolostone reservoirs due to the abundance and coexistence of sulfate and hydrocarbons, as well as the high burial temperatures (from >120 to 220 ºC) (Cai et al., 2004; Li et al., 2005; Hao et al., 2008; Liu et al., 2013; Cai et al., 2014; Jiang et al., 2014a; Liu et al., 2014; Hao et al., 2015; Jiang et al., 2015c). Calcite-4, characterized by a wide range of broadly negative carbon isotope values (Fig. 13), is interpreted to be the main mineral product of TSR. TSR can be subdivided into oil- and gas-TSR by the different hydrocarbons dominant during different temperature ranges during burial (Jiang et al., 2014a). Oil-TSR occurred at temperatures between 110 and 180 ºC, whereas gas-TSR commenced at a temperature of about 140 ºC and continued to the highest burial temperature, at about 220 ºC, as evidenced by the aqueous fluid inclusion temperature data (Fig. 11C). Quartz, celestite, and anhydrite precipitated during the TSR diagenesis stage (Fig. 15B). Bitumen also likely formed due to oil cracking and TSR. Post-TSR diagenetic processes were dominated by bitumen-free, fracture-filling calcite (calcite-5). Localized growth of celestite, barite and anhydrite in fractures only occurred in dolostone reservoirs (Fig. 15).

5.2. Calcite cementation and porosity-loss in lime-grainstone

Porosity-occlusion by calcite cementation in limestone is approximately the same as the volume of total intergranular and intragranular cements (Table 1, Fig. 10). The measured porosity in the 28 lime-grainstone samples is very low, with an average of 1.8 %, mainly due to relatively early calcite (calcite-1, and calcite-2) cementation as well as late calcite-3 cementation. Only a few single-phase fluid inclusions were found, suggesting low precipitation temperatures (less than 50ºC) (Goldstein and Reynolds, 1994a). In contrast, late calcite cements (calcite-3) precipitated at relatively higher temperatures, lying between 70 and 120 ºC (Fig. 11A). The source for these early types of calcite (calcite-1 and calcite-2) was a seawater-derived fluid, as indicated by their seawater-like strontium isotope values (Fig. 13a, Fig. 14a), whereas late diagenetic calcite

(calcite-3) was most likely sourced from the dissolution of pre-existing calcite grains and cements. Ooids in limestone commonly exhibit point- and line-contacts (pressure-induced dissolution), which, together with the abundance of stylolites, suggest that calcite cementation and porosity-loss was due to the combined effects of mechanical compaction, chemical compaction by intergranular pressure solution and cementation (Heydari, 2000). Negative shifts of $\delta^{13}C$ and $\delta^{18}O$ isotopes in some calcite cements could either be the result of freshwater influx or indicative of high-temperature diagenetic environments during calcite precipitation. However, the very low water salinities (~ 0 w.t. %), as revealed by fluid inclusion ice melting temperature measurements, confirm that localized meteoric water probably penetrated into the limestone during relative early diagenesis (<50ºC).

5.3. Impact of early dolomitization and oil charge on reservoir quality

In contrast to lime-grainstone in these reservoirs, early calcite cementation is significantly less common in dolo-grainstones and thus the visible porosity is much higher than that of limestones (Table 1, Fig. 10B). For the 44 point-counted dolostone samples, the average present-day porosity is 9.7 % (ranging from 0 to 33 %), and the average volume percentages of major cement types are listed in Table 1 and Figure 10B that reveal negligible early calcite cement but 8.6 % early dolomite cement. Previous studies have shown that sucrosic dolostone reservoirs in the Feixianguan Formation (mainly consisting of dolomite-2) have much better reservoir quality (both porosity and permeability) than the limestone reservoirs (Fig. 10) (Ma et al., 2008a; Cai et al., 2014; Wang et al., 2015). The majority of the dolomite cements (dolomite-1 and dolomite-2) were interpreted to have formed by reflux dolomitization during relatively early diagenetic processes in the Feixianguan Formation (Zhao et al., 2005; Jiang et al., 2013; Jiang et al., 2014b). Early dolomitization prevented C2 calcite cementation, which is probably the key to the creation of good dolostone reservoir quality in dolostone (Zhao et al., 2005; Jiang et al., 2014b). Finally, the preservation of porosity in dolostones can also be attributed, in part, to the elevated resistance to mechanical and chemical compaction during burial compared to the Feixianguan limestone that commonly has more stylolites and shows sutured contacts between ooids (Fig. 10) (Schmoker and Halley, 1982). In addition, oil charge appears to be a relatively early event in these dolomitized carbonate reservoirs (Hao et al., 2008; Ma et al., 2008a; Cai et al., 2010). An early oil charge can inhibit calcite cementation in oil leg, resulting in a preservation of carbonate reservoir quality during burial diagenesis, whereas intense calcite cementation filled most of the macroporosity in the water leg (Neilson et al., 1998; Cox et al., 2010).

5.4. Thermochemical sulfate reduction impact on carbonate reservoir

Thermochemical sulfate reduction (TSR) has been shown to be prevalent in the Feixianguan Formation (Cai et al., 2004; Zhu et al., 2005; Hao et al., 2008; Jiang et al., 2015c). TSR-derived calcite in the Feixianguan Formation commonly shows relatively high temperatures (> 110°C) (Fig. 11), and is characterized by low $\delta^{13}C$ and $\delta^{18}O$ values (Fig. 13) (Li et al., 2012; Cai et al., 2014; Jiang et al., 2015a; Jiang et al., 2015c). Simplified stoichiometric TSR reactions between anhydrite and the two simplest hydrocarbons can be written as follows:

$$CaSO_4 + CH_4 \rightarrow CaCO_3 + H_2S + H_2O \qquad (R2)$$

$$2CaSO_4 + C_2H_6 \rightarrow 2CaCO_3 + H_2S + 2H_2O + S \qquad (R3)$$

$$7CaSO_4 + 4C_2H_6 \rightarrow 7CaCO_3 + 7H_2S + 5H_2O + CO_2 \qquad (R4)$$

Two recent studies investigated the impact of TSR on the reservoir quality of Feixianguan Formation dolostone (Cai et al., 2014; Hao et al., 2015). Based on detailed geochemical and petrological studies, Cai et al. (2014) reported evidence for (i) anhydrite dissolution and partial filling of secondary pores by calcite, and (ii) late dolomite dissolution, and suggested that TSR was responsible for a positive effect on the formation of good dolostone reservoirs. In contrast, Hao et al. (2015) suggested that calcite cement growth, rather than dolomite dissolution, dominated TSR diagenesis in the Feixianguan Formation, and concluded that TSR had an insignificant role in altering the reservoir quality of these dolostones. It has been proposed that late diagenesis, including TSR, is not able to enhance porosity and permeability because of the low degree of water-rock interaction and the assumption that formation water is always saturated with respect to carbonate minerals in these environments (Heydari, 1997; Machel and Buschkuehle, 2008; Ehrenberg et al., 2012). However, TSR has the potential for the generation of porosity since there is a net solid volume decrease when calcite replaces anhydrite as shown in R2-R4 (note that anhydrite has a molar volume of 46 cm^3 and calcite has a molar volume of 36.9 cm^3) (Smyth and McCormick, 1995).

In the Feixianguan Formation, anhydrite is the dominate sulfate source for TSR (e.g. R2-R4), and the prominent negative shift of $\delta^{13}C$ (from ~2.5‰ down to ~-20‰) in calcite-4 suggests there was a substantial contribution of $\delta^{12}C$-enriched carbon most likely sourced from hydrocarbon (e.g. R4) during TSR (Fig. 13B) (Cai et al., 2003; Hao et al., 2008; Cai et al., 2010; Li et al., 2012; Cai et al., 2014; Jiang et al., 2014a; Hao et al., 2015; Jiang et al., 2015a; Jiang et al., 2015c). Hence, although porosity resulted from anhydrite dissolution during TSR, some, or even much, of this porosity was then filled by calcite cement (calcite-4). While some of the present solution-enlarged porosity has contributed to primary porosity (e.g. interparticle) and early diagenetic porosity (e.g.

oomoldic), our petrographic observations suggest that there is a substantial amount of pore space, e.g. solution-enlarged pores (Figs. 7C, D), that were most likely related to TSR diagenesis. Dissolution-porosity related to TSR seems to have been underestimated by Hao et al. (2015), possibly because they did not undertake a full analysis of the paragenetic sequence and did not differentiate TSR calcite from pre-TSR and post-TSR types of calcite, and the various stages of dissolution, as defined in this study (Fig. 15).

Recent studies have shown that significant amounts of fresh water were generated and added to the Feixianguan Formation during TSR (Jiang et al., 2015c), in the Permian Khuff Formation from Abu Dhabi (Worden et al., 1996), and in the Devonian fields from Western Canada Sedimentary Basin (Yang et al., 2001). The generation of fresh water due to TSR locally dilutes the pre-existing saline residual formation water by a factor of about four in the Feixianguan Formation (Fig. 12B), and possibly caused some dissolution of carbonates due to the formation water being undersaturated with respect to carbonates during TSR (Jiang et al., 2015c).

In addition, TSR produced native sulfur and pyrite (Fig. 8C), which commonly grew at the edge of non-selective, dissolution-enlarged pores. Pyrite formed during TSR due to either reaction (R5) or (R6) (Liu et al., 2013; Jiang et al., 2014a; Liu et al., 2014).

$$Fe^{2+} + 2H_2S \rightarrow FeS_2 + H_2 + 2H^+ \qquad (R5)$$

$$FeCO_3 + 2H_2S \rightarrow FeS_2 + CO_2 + H_2O + H_2 \qquad (R6)$$

The volume of pyrite in the Feixianguan Formation ranges from 0 % to 4 % (average at 0.4 %) (Table 2). The acidity of diagenetic fluids probably was transiently increased due to the release of H^+, at least near to the site of pyrite precipitation. As a consequence, carbonate dissolution may have occurred during, and after, pyrite precipitation (Figs. 7C, D). TSR calcite (calcite-3) was not observed in close association with pyrite and native sulfur. This probably suggests that during TSR, formation water may have been locally transported away from the reaction site. The precipitation rate of calcite is much slower than that for pyrite (Worden et al., 2000). It is thus possible that dissolved (TSR) calcite was transported to other parts of the Feixianguan dolostone reservoirs via diffusion, and fractures and/or faults formed by local tectonic movements (Ma et al., 2008b). Moreover, H^+ released from small volumes of pyrite precipitation may have enhanced reaction of anhydrite with dolomite and methane (Cai et al., 2014):

$$CaMg(CO_3)_2 + CaSO_4 + CH_4 + 2H^+ \rightarrow CaCO_3 + H_2S + Mg^{2+} + Ca^{2+} + 2HCO_3^- + H_2O \qquad (R7)$$

The reactions (R2-4 and R7) may result in dissolution or replacement of anhydrite and dolomite by TSR calcite, leading to an enhancement or redistribution of porosity.

In addition, high concentration of H_2S in these natural gas dolostone reservoirs may have led to present-day porosity that is 2% higher than if TSR had not happened, due to deep burial dissolution of dolomite (Ma et al., 2007). The gas-phase CO_2 in sour dolostone reservoirs has high $\delta^{13}C$ compared to CO_2 derived from oxidation of hydrocarbon since the carbon in CO_2 was, at least partly, derived from dissolved carbonate minerals during or after TSR (Huang et al., 2012; Cai et al., 2014; Hao et al., 2015). CO_2 $\delta^{13}C$ data therefore suggest that significant rock dissolution has occurred and ^{13}C-rich CO_2 was added to the reservoir fluids, during and after TSR (Liu et al., 2013).

TSR may also have increased fluid pressure by the generation of H_2S and CO_2. For example, reaction R3 shows the conversion of four moles of ethane into a combination of seven moles of H_2S and one mole of CO_2, as well as five moles of water. The resulting increase in fluid pressure at the site of TSR may have driven the diagenetic (calcite-saturated) aqueous fluids out of the TSR site to help dissipate the locally elevated pressure. This proposal is supported by a detailed fluid inclusion study of TSR diagenetic minerals and pressure modelling (Liu et al., 2006). Hence, it is possible that a complex cycling of fluids on a reservoir scale occurs during TSR, resulting in some zones of reservoir developing higher porosity whereas others are occupied by TSR calcite cements. It is interesting to note that a modelling study of TSR in the Western Canada Sedimentary Basin also concluded that TSR probably increased the overall porosity by about 1 to 2 % due to the dissolution of anhydrite and partial infilling by calcite (Hutcheon et al., 1995).

We can summarize the impact of TSR on reservoir quality in the Feixianguan Formation as: i) about 2 % net porosity was gained by a combination of dissolution of anhydrite and precipitation of calcite due to TSR; ii) the generation of TSR water may have caused some local dissolution and created additional secondary porosity; iii) further dissolution of carbonate minerals occurred due to the release of H^+ associated with pyrite precipitation; and iv) locally overpressured fluids that may have resulted from the movement of calcite-saturated water away from the TSR site.

5.5. Intra-reservoir heterogeneity

Carbonate reservoir quality in the Feixianguan Formation is controlled both by sedimentary facies and diagenetic processes (Zhao et al., 2005; Ma et al., 2008a; Cai et al., 2014; Jiang et al., 2014a; Chen et al., 2015;

Qiao et al., 2016). Good quality reservoirs are most commonly found in high-energy shoal facies and platform interior shoals that are associated with evaporites (Table 3). A large degree of reservoir quality heterogeneity is found in these carbonate reservoirs in each facies despite common initial environments of deposition (Table 3). The heterogeneity is a consequence of the diagenetic modification of pore space either by mineral dissolution or precipitation during diagenesis.

In order to better understand of how diagenesis affects intra-reservoir heterogeneity, limestone and dolostone samples from high-energy depositional environments (e.g. platform margin shoal, platform interior shoal) were examined in this study. The results shows that, despite the similar high-energy depositional environments, porosity in dolo-grainstone is high (from 0 to 33%, average at 9.7%) compared to their lime-grainstone counterparts (average of 2.1% ranging from 0 to 10%,) (Table 1). The average porosity of the platform interior shoal and platform margin shoal in dolostone is much better than the limestone (Table 3). Hence, diagenesis, and most importantly dolomitization, is the dominant factor which controls secondary porosity development and primary porosity preservation (Sun, 1995). Some parts of the dolostone reservoir are enriched in dissolution-enlarged pores whereas other parts are heavily cemented by calcite; this suggests that late diagenesis (e.g. TSR) may be able to modify the pore system by increasing the intra-reservoir heterogeneity.

5.6. Reservoir evolution model for the Feixianguan Formation

Based on petrological and geochemical studies, point counting data (Table 4), and fluid geochemistry (Ma et al., 2008b; Cai et al., 2014; Hao et al., 2015), we have synthesised a geological and porosity evolution model of the Feixianguan Formation for both the non-reservoir limestone (Fig. 16) and the dolostone reservoir (Fig. 17). The differences in reservoir quality of the dolo-grainstone and lime-grainstone is a direct consequence of their different diagenetic pathways. Marine diagenesis (calcite-1) occurred both in lime-grainstone and dolo-grainstone, and occluded an average of ~8.5% primary porosity. The conditions that led to the formation of high quality dolostone reservoir are: early dolomitization and oil charging, dissolution caused by various types of fluids such as dolomitization water, organic acids, acidic fluids generated due to TSR, uplifting and fracture formation (Jiang et al., 2014a). We have subdivided the evolution of limestone and dolostone reservoir quality in the Feixianguan Formation into three and four stages, respectively. Porosity evolution was achieved by the average point count data for each component in the lime-grainstone and dolo-grainstone during diagenetic processes (Table 1), assuming that each component has the same volume change by increased pressure and temperature.

5.6.1 Limestone reservoir evolution model

Stage 1: Meteoric water dissolution and cementation in limestone

Stage 1 for limestone consists of phases 2 and 6 (calcite-1 and calcite-2) (see Figs. 15A, 16). Based on published values, we here have assumed that the original porosity of the oolitic limestone was about 52 % (Enos and Sawatsky, 1981; Schmoker and Halley, 1982; Heydari, 2000), and initial formation water was Feixianguan seawater with salinity of about 3.5 wt. % NaCl. Marine diagenesis and calcite-1 cementation (8.5%; Table 1) resulted in the decrease of porosity to ~43.5 % (the original 52% less 8.5% of calcite-1). Meteoric water influx resulted in some moldic pores by dissolution and a decrease of formation water salinity down to 0 wt. % NaCl (Fig. 16a). Dissolution induced by meteoric water locally created some moldic pores in the limestone, although the precipitation of calcite-2 (15.25%; Table 1) decreased reservoir porosity to 28.3% due to growth of 15.25% calcite-2.

Stage 2: Mechanical compaction, pressure solution, and calcite cementation in limestone

Stage 2 consists of phases 7 to 10 (Figs. 4A, 16). Point- and line-contact relationships between ooid grains in limestone are very common. Some porosity was lost at this stage due to calcite cementation, mechanical compaction, and pressure solution, causing growth of 20.8% calcite-3 (Table 1) resulting in porosity of 7.5% (Table 1). The precipitation of small quantities of dolomite-3 (2.9%) and quartz (0.5%) cement (Table 1) further decreased the average porosity to about 4.1%. Oil charging locally occurred with some bitumen occupying the pore spaces thus decreasing the average porosity to about 0.9%. Note that TSR did not occur in the lime-grainstones.

Stage 3: Post-TSR calcite cementation and dissolution

Stage 3 in limestone consists of phases 20 to 23 (Figs. 15A, 16). This stage was dominated by calcite-5 cementation in fractures. The overall porosity decreased by ~1.2% (Table 1), thus accounting for the current average core analysis porosity of oolitic limestones in the Feixianguan Formation being now about 2% (Fig. 16).

5.6.2 Dolostone reservoir evolution model

Stage 1: Early dolomitization and moldic porosity formation

Stage 1 consists of phases 2 to 7 (Figs. 15B, 17). As for the limestones, we have assumed that the initial porosity of the original oolitic limestone was about 52% and we have assumed that, as for the limestones, growth of 8.5% marine calcite-1 cementation decreased porosity to 43.5% (i.e. 52 % less 8.5 %). Initial formation water salinity was about 3.5 wt. % NaCl; the same as for the limestone. Early reflux of evaporated and/or normal seawater resulted in dolomitization of the detrital carbonate materials and the early calcite cement (calcite-1). This phase of dolomitization may have produced some moldic pores by dissolution (Melim et al., 2001; Jiang et al., 2014b; Saller et al., 2014) and led to an increase of the formation water salinity up to 18 wt. % NaCl (Fig. 16B), although we note that molds can also be formed by marine pore fluids and meteoric water diagenesis (Melim et al., 2001). Some porosity was lost at this stage due to anhydrite cementation and mechanical compaction, resulting in a net average porosity of 32%, as supported by point counting data (grain + matrix + calcite-1; Table 1). Dolomite-1 and dolomite-2 cementation (~8.5%) further decreased the average porosity to ~23.5% (Table 1; Fig. 16b).

Stage 2: Early oil charge

Stage 2 consists of phases 8 to 13 (Figs. 15B, 17). Burial dolomitization resulted in 6.5% dolomite cementation and replacement (dolomite-3) decreasing the average porosity to about 17 % (23.5 % less 6.5 %) (Fig. 17). Calcite-3 and other diagenetic minerals (e.g. barite, fluorite, quartz, celestite, and pyrite) represent small volumes (< 0.5 %) (Table 1) and so led to a small net reduction in porosity down to about 16 % (Fig. 17) due to compaction and pressure solution. Early oil, sourced from Lower Permian strata, then charged the Feixianguan dolostone reservoirs and maintained the porosity by inhibiting further cementation (e.g., calcite) in oil saturated reservoir part (Neilson et al., 1998; Heasley et al., 2000; Worden et al., 2000; Cai et al., 2010; Cox et al., 2010; Sathar et al., 2012). Hence, early oil charge had a positive effect on reservoir quality in the carbonate reservoirs (Ma et al., 2008b; Saller et al., 2014; Hao et al., 2015).

Stage 3: TSR dissolution and cementation, gas charge, and bitumen formation

Stage 3 consists of phases 14 to 19 (Figs. 15B, 17). TSR is the dominant diagenetic event in this stage. TSR resulted in anhydrite dissolution and calcite precipitation, and produced significant amounts of H_2S and CO_2. Dissolution-enlarged pores in the Feixianguan Formation are most likely related to TSR, and the overall TSR-induced porosity-increase was ~2%, as discussed previously. TSR locally increased visible porosity by up to one third in some vin thin-sections (Table 1). However, calcite-4, pyrite, and bitumen have occupied about

1.6%, 0.4%, and 5% of the total rock volume in grain-dolostone reservoirs, respectively (Table 1). Hence, following TSR and bitumen generation, the average porosity in the Feixianguan was ~11% (Fig. 17).

Stage 4: Post-TSR calcite cementation and dissolution

Stage 4 consists of phases 20 to 23 (Figs. 15B, 17). This stage is dominated by calcite-5 cementation and TSR induced dissolution of carbonate minerals, although some other minerals, such as anhydrite, celestite and barite, locally precipitated in fractures. The overall porosity decreased by ~1% (Table 1), thus the current average core analysis porosity of oolitic dolostones in the Feixianguan Formation is about 10% (Fig. 17).

5.7. Implications for ooid-dominated dolo-grainstone reservoir evolution during diagenesis

This detailed, inter-well-scale study of contrasting diagenesis between ooid-dominated lime-grainstone and dolo-grainstone reservoirs has enabled us to reconstruct the diagenetic fluid and porosity evolution of carbonates deposited in a tidal-dominated platform-marginal oolitic shoal complex. Previous studies of the diagenetic and reservoir evolution in the Feixianguan Formation focused on the dolostone showing good reservoir quality, and did not emphasize the diagenesis of their limestone counterpart (Zhao et al., 2005; Huang et al., 2007; Ma et al., 2008a; Chen et al., 2015; Hao et al., 2015; Wang et al., 2015). Detailed comparison and analysis of diagenetic sequences, fluid inclusion homogenization temperatures and salinities of the diagenetic minerals, $\delta^{13}C$, $\delta^{18}O$, $^{87}Sr/^{86}Sr$ of carbonate minerals, porosity and diagenetic mineral quantitative volume estimations, have together allowed us to develop a comprehensive understanding of the heterogeneous evolution of carbonate diagenesis and reservoir quality.

Deeply buried (> 3,500 m) carbonate successions generally show relatively low porosity and permeability due to mechanical compaction, pressure dissolution, and calcite and dolomite cementation (Schmoker and Halley, 1982; Heydari, 2000; Ehrenberg et al., 2006). This study suggests that diagenesis, most importantly early dolomization and thermochemical sulfate reduction, have yielded reservoirs with significant porosity in the Feixianguan Formation from the Sichuan Basin in China.

Ooid-dominated grainstones globally represent many important carbonate reservoirs (Harris and Weber, 2006; Lehrmann et al., 2012): e.g., Mississippian Formation of the United States (Handford, 1988), the Triassic Khuff and Kangan Formations (Moradpour et al., 2008; Faqira et al., 2009), and the Jurassic Arab Formation (Lindsay et al., 2006; Ehrenberg et al., 2007). These have similar geological settings and show reservoir characteristics comparable to those of the Feixianguan Formation. Dolomitization occurred in evaporitic sabkha and shallow reflux settings associated with anhydrite cementation. Removal of anhydrite and the generation of H_2S and low salinity water, during later diagenesis caused by sulfate reduction reactions. Both bacterial sulfate reduction (BSR) in relatively lower temperatures (< 100 °C) (Saller et al., 2014) and thermochemical sulfate reduction (TSR) in relatively high temperatures (> 100 °C) (Jiang et al., 2015c), are able to locally enhance the reservoir quality. Hence, the diagenetic and reservoir formation model of the ooid-dominated dolo-grainstone of the Feixianguan Formation may be applicable to other deeply buried dolo-grainstone reservoirs deposited in similar sedimentary facies (e.g. Triassic Khuff and Kangan Formations on the Arabian plate, Mississippian Formation of the United States, and the Jurassic Arab Formation).

6. Conclusions

(1) Integration of petrographic, isotopic, fluid inclusion, and porosity point counting data, reveals discrete diagenetic and porosity evolution patterns in limestone and dolostone reservoirs in the Lower Triassic Feixianguan Formation.

(2) Early calcite cementation and mechanical compaction, pressure solution, and late stage calcite cementation have reduced porosity in limestone to ~2%. Negative trend of $\delta^{18}O$ and the low salinity data (<3.5 wt. %) of some calcite-2 and calcite-3 in limestone suggest that there was an influx of meteoric water.

(3) Dolostone reservoirs have retained relatively high porosity (~10 %) mainly due to four important diagenetic stages (pre-TSR, oil charge, TSR, and post-TSR) that have collectively controlled reservoir quality.

(4) Average porosity in oolitic dolostone was ~23.5% after early dolomitization. Early dolomitization appears to be crucial in the formation of dolostone reservoirs. The reservoir quality of dolostones is significantly higher than that of limestones mainly due to: i) the generation of new porosity instead of calcite cementation, and ii) dolostone being more resistant to compaction than limestone.

(5) Early oil charge had a positive effect on dolostone reservoir quality which is able to inhabit calcite cement growth into the pore spaces in the oil leg. Subsequent diagenesis of dolostone reservoirs was dominated by thermochemical sulfate reduction (TSR). The depleted $\delta^{13}C$ (~-20‰ VPDB) and $\delta^{18}O$ values of deep diagenetic carbonates (calcite-4), the elevated precipitation temperatures (>110°C), and the presence of native sulfur and

pyrite, suggest that these minerals are the products of TSR processes. TSR was responsible for the formation of enlarged dissolution pores that enhanced the reservoir quality (increased porosity by ~2 %) in dolostones.

(6) The mechanisms by which TSR improved dolostone reservoir quality are: i) anhydrite dissolution; ii) production of significant amounts of water (dilution of initially saline formation water in the gas leg by TSR-induced fresh water by a factor of four); iii) generation of H_2S, CO_2, and the reaction of H_2S with Fe^{2+} (with the iron found in ferroan calcite and ferroan dolomite) that created acidic fluids capable of causing a further amount of dissolution. The overall impact of post-TSR diagenesis on dolostone reservoir was largely insignificant.

(7) This study has demonstrated the importance of early dolomitization and late TSR in the preservation of reservoir quality in deeply buried dolostones and the destruction of pores in equivalent limestones, both of which were deposited in platform interior shoal and margin shoal facies. Dolostone represents much better reservoir quality than limestone due to the preservation of porosity and the creation of secondary pores largely resulting from TSR that was localised to the anhydrite-bearing dolostone. The study of diagenesis and porosity evolution in platform interior and margin shoal facies from Feixianguan Formation may be applicable to other deeply buried dolo-grainstone reservoirs that have intra-reservoir heterogeneity deposited in similar sedimentary facies.

Acknowledgements

This work has been financially supported by the Natural Science Foundation of China (Grant Nos. 41402132 and 41672143) and a scholarship under the International Postdoctoral Exchange Fellowship Program (GrantNo. 20150035) supported by the Office of China Postdoctoral Council (OCPC). The authors are especially grateful for critical and constructive reviews by two anonymous reviewers who have greatly improved the manuscript. This paper has also benefited from detailed comments and instructions from Marine and Petroleum Geology editors Dr. Massimo Zecchin and Dr. Enrique Gomez-Rivas.

References

Bildstein, O., Worden, R.H., Brosse, E., 2001. Assessment of anhydrite dissolution as the rate-limiting step during thermochemical sulfate reduction. Chemical Geology 176, 173-189.

Cai, C.F., He, W.X., Jiang, L., Li, K.K., Xiang, L., Jia, L.Q., 2014. Petrological and geochemical constraints on porosity difference between Lower Triassic sour-and sweet-gas carbonate reservoirs in the Sichuan Basin. Marine and Petroleum Geology 56, 34-50.

Cai, C.F., Li, K.K., Zhu, Y.M., Xiang, L., Jiang, L., 2010. TSR origin of sulfur in Permian and Triassic reservoir bitumen, East Sichuan Basin, China. Organic Geochemistry 41, 871-878.

Cai, C.F., Worden, R.H., Bottrell, S.H., Wang, L.S., Yang, C.C., 2003. Thermochemical sulphate reduction and the generation of hydrogen sulphide and thiols (mercaptans) in Triassic carbonate reservoirs from the Sichuan Basin, China. Chemical Geology 202, 39-57.

Cai, C.F., Xie, Z.Y., Worden, R.H., Hu, G.Y., Wang, L.S., He, H., 2004. Methane-dominated thermochemical sulphate reduction in the Triassic Feixianguan Formation East Sichuan Basin, China: towards prediction of fatal H_2S concentrations. Marine and Petroleum Geology 21, 1265-1279.

Chen, P.Y., Tan, X.C., Yang, H.T., Tang, M., Jiang, Y.W., Jin, X.J., Yu, Y., 2015. Characteristics and genesis of the Feixianguan Formation oolitic shoal reservoir, Puguang gas field, Sichuan Basin, China. Frontiers of earth science 9, 26-39.

Choquette, P.W., Pray, L.C., 1970. Geologic nomenclature and classification of porosity in sedimentary carbonates. American Association of Petroleum Geologists Bulletin 54, 207-250.

Cox, P.A., Wood, R.A., Dickson, J.A.D., Al Rougha, H.B., Shebl, H., Corbett, P.W.M., 2010. Dynamics of cementation in response to oil charge: evidence from a Cretaceous carbonate field, UAE. Sedimentary Geology 228, 246-254.

Davies, G.R., Smith, L.B., 2006. Structurally controlled hydrothermal dolomite reservoir facies: An overview. American Association of Petroleum Geologists, Bulletin 90, 1641-1690.

Dickson, J., 1966. Carbonate identification and genesis as revealed by staining. Journal of Sedimentary Research 36, 491-505.

Dickson, J.A.D., Kenter, J.A.M., 2014. Diagenetic Evolution of Selected Parasequences Across A Carbonate Platform: Late Paleozoic, Tengiz Reservoir, Kazakhstan. Journal of Sedimentary Research 84, 664-693.

Ehrenberg, S.N., Eberli, G.P., Keramati, M., Moallemi, S.A., 2006. Porosity-permeability relationships in interlayered limestone-dolostone reservoirs. American Association of Petroleum Geologists, Bulletin 90, 91-114.

Ehrenberg, S.N., Nadeau, P.H., Aqrawi, A.A.M., 2007. A comparison of Khuff and Arab reservoir potential throughout the Middle East. AAPG bulletin 91, 275-286.

Ehrenberg, S.N., Walderhaug, O., Bjørlykke, K., 2012. Carbonate porosity creation by mesogenetic dissolution: Reality or illusion? American Association of Petroleum Geologists, Bulletin 96, 217-233.

Enos, P., Sawatsky, L., 1981. Pore networks in Holocene carbonate sediments. Journal of Sedimentary Research 51, 961-985.

Faqira, M.I., Bakhiet, A.F., Tang, D.Z., Tan, W., Ahmed, A., 2009. A Review of the Permo-Triassic Gas Play in the Arabian Gulf Region, in: Poppelreiter, M.C. (Ed.), 2009 AAPG Annual convention and Exhibition, Denver, Colorado, USA, The Netherlands, pp. 163-198.

Goldstein, R.H., Reynolds, T.J., 1994a. Systematics of fluid inclusions in diagenetic minerals: SEPM Short Course Notes, 31. 199.

Goldstein, R.H., Reynolds, T.J., 1994b. Systematics of Fluid Inclusions in Diagenetic Minerals: SEPM, Short Course 31. 199.

Guo, T.L., 2010. Diagenesis of the Feixianguan oolitic shoal reservoirs in the northeastern Sichuan Basin-examples from Xuanhan-Daxian and Yuanba areas. Oil & Gas Geology 31, 620-631. (in chinese with English abstract).

Handford, C.R., 1988. Review of carbonate sand-belt deposition of ooid grainstones and application to Mississippian reservoir, Damme Field, southwestern Kansas. AAPG Bulletin 72, 1184-1199.

Hao, F., Guo, T.L., Zhu, Y.M., Cai, X.Y., Zou, H.Y., Li, P.P., 2008. Evidence for multiple stages of oil cracking and thermochemical sulfate reduction in the Puguang gas field, Sichuan Basin, China. American Association of Petroleum Geologists, Bulletin 92, 611.

Hao, F., Zhang, X.F., Wang, C.W., Li, P.P., Guo, T.L., Zou, H.Y., Zhu, Y.M., Liu, J.Z., Cai, Z.X., 2015. The fate of CO2 derived from thermochemical sulfate reduction (TSR) and effect of TSR on carbonate porosity and permeability, Sichuan Basin, China. Earth-Science Reviews 141, 154-177.

Harris, P.M., Weber, L.J., 2006. Giant hydrocarbon reservoirs of the world: From rocks to reservoir characterization and modeling. 88. AAPG Memoir, 469.

Heasley, E.C., Worden, R.H., Hendry, J.P., 2000. Cement distribution in a carbonate reservoir: recognition of a palaeo oil–water contact and its relationship to reservoir quality in the Humbly Grove field, onshore, UK. Marine and Petroleum Geology 17, 639-654.

Heydari, E., 1997. The role of burial diagenesis in hydrocarbon destruction and H2S accumulation, Upper Jurassic Smackover Formation, Black Creek Field, Mississippi. American Association of Petroleum Geologists, Bulletin 81, 26-45.

Heydari, E., 2000. Porosity loss, fluid flow, and mass transfer in limestone reservoirs: Application to the upper Jurassic Smackover formation, Mississippi. American Association of Petroleum Geologists, Bulletin 84, 100-118.

Hiemstra, E.J., Goldstein, R.H., 2015. Repeated injection of hydrothermal fluids into downdip carbonates: a diagenetic and stratigraphic mechanism for localization of reservoir porosity, Indian Basin Field, New Mexico, USA. Geological Society, London, Special Publications 406, 141-177.
Hill, C., 1995. Sulfur redox reactions: hydrocarbons, native sulfur, Mississippi Valley-type deposits, and sulfuric acid karst in the Delaware Basin, New Mexico and Texas. Environmental Geology 25, 16-23.
Huang, S.J., Huang, K.K., Lü, J., Lan, Y.F., 2012. Carbon isotopic composition of Early Triassic marine carbonates, Eastern Sichuan Basin, China. Science China Earth Sciences 55, 2026-2038.
Huang, S.J., Qing, H.R., Hu, Z., Zou, M., Feng, W., Wang, C., Gao, X., Wang, Q., 2007. Influence of sulfate reduction on diagenesis of Feixianguan carbonate in Triassic, NE Sichuan Basin of China. Acta Sedimentologica Sinica 25, 815-824.
Hugman III, R., Friedman, M., 1979. Effects of texture and composition on mechanical behavior of experimentally deformed carbonate rocks. American Association of Petroleum Geologists, Bulletin 63, 1478-1489.
Hutcheon, I., Krouse, H.R., Abercrombie, H.J., 1995. Controls on the origin and distribution of elemental sulfur, H_2S, and CO_2 in paleozoic hydrocarbon reservoirs in Western Canada, in: Vairavamurthy, M.A., Schoonen, M.A.A. (Eds.), Geochemical Transformations of Sedimentary Sulfur, pp. 426-438.
Jiang, L., Cai, C.F., Worden, R.H., Crowley, S.F., Jia, L.Q., Zhang, K., Duncan, I.J., 2016. Multiphase dolomitization of deeply buried Cambrian petroleum reservoirs, Tarim Basin, north-west China. Sedimentology 63, 2130-2157.
Jiang, L., Cai, C.F., Worden, R.H., Li, K.K., Xiang, L., 2013. Reflux dolomitization of the Upper Permian Changxing Formation and the Lower Triassic Feixianguan Formation, NE Sichuan Basin, China. Geofluids 13, 232-245.
Jiang, L., Cai, C.F., Worden, R.H., Li, K.K., Xiang, L., Chu, X.L., Shen, A.J., Li, W.J., 2015a. Rare earth element and yttrium (REY) geochemistry in carbonate reservoirs during deep burial diagenesis: Implications for REY mobility during thermochemical sulfate reduction. Chemical Geology 415, 87-101.
Jiang, L., Pan, W.Q., Cai, C.F., Jia, L.Q., Pan, L.Y., Wang, T.K., Li, H.X., Chen, S.L., Chen, Y., 2015b. Fluid mixing induced by hydrothermal activity in the Ordovician carbonates in Tarim Basin, China. Geofluids 15, 483-498.
Jiang, L., Worden, R.H., Cai, C.F., 2014a. Thermochemical sulfate reduction and fluid evolution of the Lower Triassic Feixianguan Formation sour gas reservoirs, northeast Sichuan Basin, China. American Association of Petroleum Geologists, Bulletin 98, 947-973.
Jiang, L., Worden, R.H., Cai, C.F., 2015c. Generation of isotopically and compositionally distinct water during thermochemical sulfate reduction (TSR) in carbonate reservoirs: Triassic Feixianguan Formation, Sichuan Basin, China. Geochimica et Cosmochimica Acta 165, 249-262.
Jiang, L., Worden, R.H., Cai, C.F., Li, K.K., Xiang, L., Cai, L.L., He, X.Y., 2014b. Dolomitization of Gas Reservoirs: The Upper Permian Changxing and Lower Triassic Feixianguan Formations, Northeast Sichuan Basin, China. Journal of Sedimentary Research 84, 792-815.
Koehn, D., Rood, M.P., Beaudoin, N., Chung, P., Bons, P.D., Gomez-Rivas, E., 2016. A new stylolite classification scheme to estimate compaction and local permeability variations. Sedimentary Geology 346, 60-71.
Lehrmann, D.J., Minzoni, M., Li, X.W., Yu, M.Y., Payne, J.L., Kelley, B.M., Schaal, E.K., Enos, P., 2012. Lower Triassic oolites of the Nanpanjiang Basin, south China: facies architecture, giant ooids, and diagenesis—implications for hydrocarbon reservoirs. AAPG bulletin 96, 1389-1414.
Li, J., Xie, Z., Dai, J., Zhang, S., Zhu, G., Liu, Z., 2005. Geochemistry and origin of sour gas accumulations in the northeastern Sichuan Basin, SW China. Organic Geochemistry 36, 1703-1716.
Li, K.K., Cai, C.F., Jiang, L., Cai, L.L., Jia, L.Q., Zhang, B., Xiang, L., Yuan, Y.Y., 2012. Sr evolution in the Upper Permian and Lower Triassic carbonates, northeast Sichuan basin, China: constraints from chemistry, isotope and fluid inclusions. Applied Geochemistry 27, 2409-2424.
Lindsay, R.F., Cantrell, D.L., Hughes, G.W., Keith, T.H., Mueller III, H.W., Russell, S.D., 2006. Ghawar Arab-D reservoir: widespread porosity in shoaling-upward carbonate cycles, Saudi Arabia, Harris, P.M., Weber, L.J. (Eds.) Giant Hydrocarbon Reservoirs of the World: from Rocks to Reservoir Characterization. 88. AAPG Memoir, 97-138.
Liu, D.H., Xiao, X.M., Xiong, Y.Q., Geng, A.S., Tian, H., Peng, P., Shen, J.G., Wang, Y.P., 2006. Origin of natural sulphur-bearing immiscible inclusions and H_2S in oolite gas reservoir, Eastern Sichuan. Science in China Series D-Earth Sciences 49, 242-257.
Liu, Q.Y., Worden, R.H., Jin, Z.J., Liu, W.H., Li, J., Gao, B., Zhang, D.W., Hu, A.P., Yang, C., 2013. TSR versus non-TSR processes and their impact on gas geochemistry and carbon stable isotopes in Carboniferous, Permian and Lower Triassic marine carbonate gas reservoirs in the Eastern Sichuan Basin, China. Geochimica et Cosmochimica Acta 100, 96-115.

Liu, Q.Y., Worden, R.H., Jin, Z.J., Liu, W.H., Li, J., Gao, B., Zhang, D.W., Hu, A.P., Yang, C., 2014. Thermochemical sulphate reduction (TSR) versus maturation and their effects on hydrogen stable isotopes of very dry alkane gases. Geochimica et Cosmochimica Acta 137, 208-220.

Loucks, R.G., 1999. Paleocave carbonate reservoirs; origins, burial-depth modifications, spatial complexity, and reservoir implications. American Association of Petroleum Geologists, Bulletin 83, 1795-1834.

Lucia, F.J., 1995. Rock-fabric/petrophysical classification of carbonate pore space for reservoir characterization. American Association of Petroleum Geologists, Bulletin 79, 1275-1300.

Lucia, F.J., 2004. Origin and petrophysics of dolostone pore space. Geological Society, London, Special Publications 235, 141-155.

Ma, Y.S., Guo, T.L., Zhao, X.F., Cai, X.Y., 2008a. The formation mechanism of high-quality dolomite reservoir in the deep of Puguang Gas Field. Science in China Series D-Earth Sciences 51, 53-64.

Ma, Y.S., Guo, T.L., Zhu, G.Y., Cai, X.Y., Xie, Z.Y., 2007. Simulation experimental envidence of corrosion alteration of hydrogen sulfide for carbonate resrevoirs- an example as the Feixianguan Formation in the east Sichuan. Chinses Science Bulletin 52, 136-141.

Ma, Y.S., Zhang, S., Guo, T.L., Zhu, G., Cai, X.Y., Li, M., 2008b. Petroleum geology of the Puguang sour gas field in the Sichuan Basin, SW China. Marine and Petroleum Geology 25, 357-370.

Machel, H.G., 1987. Saddle dolomite as a by-product of chemical compaction and thermochemical sulfate reduction. Geology 15, 936-940.

Machel, H.G., 2004a. Concepts and models of dolomitization: a critical reappraisal. The geometry and petrogenesis of dolomite hydrocarbon reservoirs, 7¨C63.

Machel, H.G., 2004b. Concepts and models of dolomitization: a critical reappraisal, The geometry and petrogenesis of dolomite hydrocarbon reservoirs, Braithwaite, C. J. R., Rizzi, G. & Darke, G. (eds). Geological Society, London, Special Publications 235, 7-63.

Machel, H.G., Buschkuehle, B.E., 2008. Diagenesis of the Devonian Southesk-Cairn Carbonate Complex, Alberta, Canada: Marine Cementation, Burial Dolomitization, Thermochemical Sulfate Reduction, Anhydritization, and Squeegee Fluid Flow. Journal of Sedimentary Research 78, 366.

Machel, H.G., Krouse, H.R., Riciputi, L.R., Cole, D.R., 1995. Devonian Nisku sour gas play, Canada: A unique natural laboratory for study of thermochemical sulfate reduction, in: Vairavamurthy, M.A., Schoonen, M.A.A. (Eds.), Geochemical Transformations of Sedimentary Sulfur, pp. 439-454.

Melim, L.E., Swart, P.S., Maliva, R.G., 2001. Meteoric and marine-burial diagenesis in the subsurface of Great Bahama Bank: Results of the Bahamas Drilling Project (Ed R.N. Ginsburg). SEPM Spec. Publ. 70, 137-161.

Moradpour, M., Zamani, Z., Moallemi, S., 2008. Controls on reservoir quality in the lower Triassic Kangan formation, southern Persian Gulf. Journal of Petroleum Geology 31, 367-385.

Neilson, J.E., Oxtoby, N.H., 2008. The relationship between petroleum, exotic cements and reservoir quality in carbonates–A review. Marine and Petroleum Geology 25, 778-790.

Neilson, J.E., Oxtoby, N.H., Simmons, M.D., Simpson, I.R., Fortunatova, N.K., 1998. The relationship between petroleum emplacement and carbonate reservoir quality: examples from Abu Dhabi and the Amu Darya Basin. Marine and Petroleum Geology 15, 57-72.

Qiao, Z.F., Janson, X., Shen, A.J., Zheng, J.F., Zeng, H.L., Wang, X.F., 2016. Lithofacies, architecture, and reservoir heterogeneity of tidal-dominated platform marginal oolitic shoal: An analogue of oolitic reservoirs of Lower Triassic Feixianguan Formation, Sichuan Basin, SW China. Marine and Petroleum Geology 76, 290-309.

Qing, H.R., Mountjoy, E.W., 1994. Formation of coarsely crystalline, hydrothermal dolomite reservoirs in the Presqu'ile barrier, Western Canada Sedimentary Basin. American Association of Petroleum Geologists, Bulletin 78, 55-77.

Saller, A.H., Dickson, J.A.T.D., 2011. Partial dolomitization of a Pennsylvanian limestone buildup by hydrothermal fluids and its effect on reservoir quality and performance. American Association of Petroleum Geologists, Bulletin 95, 1745-1762.

Saller, A.H., Pollitt, D., Dickson, J., 2014. Diagenesis and porosity development in the First Eocene reservoir at the giant Wafra Field, Partitioned Zone, Saudi Arabia and Kuwait. American Association of Petroleum Geologists, Bulletin 98, 1185-1212.

Sathar, S., Worden, R.H., Faulkner, D.R., Smalley, P.C., 2012. The effect of oil saturation on the mechanism of compaction in granular materials: higher oil saturations lead to more grain fracturing and less pressure solution. Journal of Sedimentary Research 82, 571-584.

Schmoker, J.W., Halley, R.B., 1982. Carbonate porosity versus depth: a predictable relation for south Florida. American Association of Petroleum Geologists, Bulletin 66, 2561-2570.

Smyth, J.R., McCormick, T.C., 1995. Crystallographic data for minerals. Mineral Physics and Crystallography: A Handbook of Physical Constants 2, 1-17.

Sun, S.Q., 1995. Dolomite reservoirs: porosity evolution and reservoir characteristics. American Association of Petroleum Geologists, Bulletin 79, 186-204.

Wang, G.W., Li, P.P., Hao, F., Zou, H.Y., Yu, X.Y., 2015. Origin of dolomite in the third member of Feixianguan Formation (Lower Triassic) in the Jiannan area, Sichuan Basin, China. Marine and Petroleum Geology 63, 127-141.
Warren, J.K., 2000. Dolomite: occurrence, evolution and economically important associations. Earth-Science Reviews 52, 1-81.
Worden, R.H., Carrigan, W.J., Jones, P.J., 2004. Origin of H_2S in Khuff reservoirs by thermochemical sulfate reduction: Evidence from fluid inclusions. Saudi Aramco Journal of Technology 43, 42-52.
Worden, R.H., Smalley, P.C., Cross, M.M., 2000. The influence of rock fabric and mineralogy on thermochemical sulfate reduction: Khuff Formation, Abu Dhabi. Journal of Sedimentary Research 70, 1210-1221.
Worden, R.H., Smalley, P.C., Oxtoby, N.H., 1995. Gas souring by thermochemical sulfate reduction at 140 degrees C. American Association of Petroleum Geologists Bulletin 79, 854-863.
Worden, R.H., Smalley, P.C., Oxtoby, N.H., 1996. The effects of thermochemical sulfate reduction upon formation water salinity and oxygen isotopes in carbonate gas reservoirs. Geochimica et Cosmochimica Acta 60, 3925-3931.
Yang, C., Hutcheon, I., Krouse, H.R., 2001. Fluid inclusion and stable isotopic studies of thermochemical sulphate reduction from Burnt Timber and Crossfield East gas fields in Alberta, Canada. Bulletin of Canadian Petroleum Geology 49, 149-164.
Zhao, W., Luo, P., Chen, G., Cao, H., Zhang, B., 2005. Origin and reservoir rock characteristics of dolostones in the Early Triassic Feixianguan Formation, NE Sichuan Basin, China: Significance for future gas exploration. Journal of Petroleum Geology 28, 83-100.
Zhou, R.Q., Fu, H., Xu, G.S., Ding, S.B., 2014. Diagenesis and types of Feixianguan Formation carbonate rock in Yuanba block of Northeast Sichuan, China. Journal of Chengdu University of Technology (Science 8-Technology Edition) 41, 733-742.
Zhu, D.Y., Meng, Q.Q., Jin, Z.J., Liu, Q.Y., Hu, W.X., 2015. Formation mechanism of deep Cambrian dolomite reservoirs in the Tarim basin, northwestern China. Marine and Petroleum Geology 59, 232-244.
Zhu, G.Y., Zhang, S.C., Liang, Y.B., Dai, J.X., Li, J., 2005. Isotopic evidence of TSR origin for natural gas bearing high H_2S contents within the Feixianguan Formation of the northeastern Sichuan Basin, southwestern China. Science in China Series D-Earth Sciences 48, 1960-1971.

Figure Caption:

Figure 1. A) Paleogeography and locations of the sampled gas fields. The Feixianguan Formation dolomite reservoirs in the NE Sichuan Basin. B) Cross section (from A to B in part A) showing stratigraphic relationships and sedimentary facies distribution of the Feixianguan and Changxing formations. Modified from Jiang et al. (2014b).

Figure 2. A) Stratigraphic and porosity correlation of the oolitic limestone and dolostone in the Feixianguan Formation across the open platform on the southwest side of Kaijiang–Liangping Bay to the restricted platform on the northwest side in Sichuan Basin (Fig. 1B). B) Core samples from well LG-001 showing the contrast reservoir quality between the dolostone section and limestone section: dolostone is porous and shows good moldic porosity whereas limestone is tight and enriched in stylolites and calcite cement. C) Core-derived porosity-permeability data of oolitic limestone reservoir in the Yuanba gas field, data modified from Cai et al. (2014). D) Core-derived porosity-permeability data of ooids enriched dolostone reservoir in the Puguang 2 well, data modified from Ma et al. (2008b).

Figure 3. Burial and paleo-temperature histories constructed of well PG2 (A) and (B) well YB2 from the East Sichuan Basin, modified from Cai et al. (2014). Isotherms were constrained by vitrinite reflectance and fluid inclusion measurements.

Figure 4. Different types of calcite cements and stylolite from the limestone in the Feixianguan Formation, well LG001, depth 6088.8 m. A) Calcite-1 and calcite-2 in limestone, open oomodic pores (red epoxy; yellow arrow) locally present, well HB2, 5,104.3m. B) Calcite-2 (in red) filling in moldic porosity and interparticle pores in limestone, well YB2, depth 6428 m. C) Photomicrograph shows tight limestone with minimal visual porosity due to the presence of stylolite (red arrow) and volumetrically-important calcite-3 cementation.

Figure 5. Different types of calcite cements precipitated in various diagenetic environments in dolostone in the Feixianguan Formation (A, B, C are photomicrograph figures, D is a photo of BSEM). A) Calcite-3 (red) filling in fracture in dolomite reservoir, well LJ1, 3,470.40 m. B) Oil-stage TSR calcite-4 (red) and bitumen (black) filling in dissolution-enlarged pores (blue proxy) in dolomite reservoir, dissolution pores locally present in calcite-3, micrite envelopes (yellow arrow) developed in the edges of ooids, well LJ2, 3,232.9m. C) Gas-stage TSR calcite-4 (red) does not contain bitumen or oil inclusions filling (black) in dissolution pores in dolomite reservoir, well LJ6, 3,936.00 m. D) Late stage post-TSR calcite-5 (light gray) filling in fractures in the dolomite reservoir, well DW102, depth 4901 m.

Figure 6. Photomicrographs showing different preservation of original ooid textures in dolomite reservoirs. A) Micro-crystalline dolomite with early replaced dolomite cement (red arrow), the original ooid texture is well persevered, white space stand for pore space, well PG2, 4977.4 m; B) Coarsely crystalline, fabric destructive dolomite, the original ooid texture cannot be discerned due to severe recrystallization, abundant intercrystalline porosity (blue) is present, well LJ2, 3,232.2 m.

Figure 7. Photomicrographs show different types of dissolution porosity in dolomite reservoirs. A) Partially dissolved moldic porosity (red) developed in ooids, well PG2, depth 5130 m. B: Open mold (red) show completely dissolution of the ooids, well PG2, depth 5133 m. C) Dissolution enlarged porosity up to millimetres range (blue) with some ooids completely dissolved, LJ2 3,232.9 m. D) Late dissolution of coarse dolomite crystals, which were partially or completely dissolved (red), locally filling with bitumen, well PG2, depth 5130 m.

Figure 8: Photomicrographs (A, B) and BSEM images (C, D) show other non-carbonate minerals in dolomite reservoirs. A) Early anhydrite cement (marked as A) filling in both interparticle and intraparticle porosities of dolostone (marked as D), well PG11, 5,818.00 m. B) Late stage quartz cement (marked as Q) filling in dissolution enlarged pores in dolostone (marked as D), well D2, depth 4300 m. C) Pyrite (marked as Py) filling in dissolution pores in dolostone (marked as D), D2-25, depth 4309 m. D) Barite (marked as Ba) associated with fluorite (marked as F) and calcite (marked as C) filling in a fracture, well P2-30.

Figure 9: Photomicrographs show three generation of fractures in dolomite reservoir. A) Fracture-1 crosscut by fracture-2, both of which were filled with calcite-3 cement, well HB2-5, depth 5105.2 m. B) Fracture-3 cross-cutting all the other minerals suggesting that it represents the latest fracture stage, and it locally remains open (red) without any mineral in-filling, well PG2, depth 5103 m.

Figure 10: Compositions of oolitic limestone (A) and oolitic dolomite (B). Original porosity in limestone was nearly completely filled by early calcite, thus limestones show negligible late diagenetic minerals or dissolution porosity. In contrast, dolostone reservoirs contain only minor quantities of early calcite cement and have much higher remaining porosity and quantities of late diagenetic minerals dominated by dolomite and bitumen.

Figure 11: Fluid-inclusion data obtained from different types of calcite in the Feixianguan Formation. A) Fluid-inclusion homogenization temperatures from aqueous inclusions from pre-TSR calcite (calcite-2). B) Salinity of aqueous inclusions from calcite-2. C) Fluid-inclusion homogenization temperatures from two-phase aqueous inclusions from TSR calcite-4 (those with oil or bitumen inclusions are oil stage TSR calcite; those without are gas stage TSR calcite). D) Salinity of aqueous inclusions from TSR calcite-4. E) Fluid-inclusion homogenization temperatures from two-phase aqueous inclusions from post-TSR calcite (calcite-5). F) Salinity of aqueous inclusions from calcite-5. Fluid inclusion data from dolostone reservoirs are adapted from Jiang et al. (2015a).

Figure 12: A) Average salinity and homogenization temperature data from fluid inclusions in calcite cements in limestone. B) Average salinity and homogenization temperature from fluid inclusions in pre-TSR, TSR, and post-TSR calcite in dolomite, adapted data from Jiang et al. (2015c).

Figure 13: Carbon and oxygen isotopic compositions of (A) limestone and (B) dolostone from the Feixianguan Formation in the NE Sichuan Basin. Dash open rectangles are adapted from previous studies (Jiang et al., 2014a; Jiang et al., 2015a; Jiang et al., 2015c); red rectangle filled with red symbols is from this study.

Figure 14: $^{87}Sr/^{86}Sr$ ratios of various types of carbonate minerals in (A) limestone and (B) dolostone, in comparison with those from literature data for coeval seawater from the Lower Triassic Feixianguan Formation in NE Sichuan Basin, China. Sr isotope and age data for the Feixianguan and Jialingjiang seawater from Jiang et al. (2014b).

Figure 15. Paragenetic sequence of A) limestone and B) dolostone in the Feixianguan Formation in northeast Sichuan Basin, summarizing major products of pre-TSR diagenesis, TSR diagenesis, post-TSR diagenesis, and the temperature for each diagenetic realms. Temperature data are from fluid inclusion analysis. Time scale bar was added by combing the burial histories in Figure 3 with fluid inclusion data.

Figure 16: Limestone reservoir evolution models for the Feixianguan Formation. The model has been divided into three different diagenetic stages, which are here considered to be important for reservoir quality evolution. Each stage has distinguishable diagenetic fluids, products, and porosity. They are: stage 1, meteoric water dissolution and cementation; stage 2, mechanical compaction, pressure solution, and calcite cementation; stage 3, post-TSR calcite cementation, see text for details of each stage. Porosity in each diagenetic stage was calculated by the average point count data of lime-grainstone and dolo-grainstone in Table 1.

Figure 17: Dolostone reservoir evolution models for the Feixianguan Formation. The models have been divided into four different diagenetic stages, which are here considered to be important for reservoir quality evolution. Each stage has distinguishable diagenetic fluids, products, and porosity. They are: stage 1, early dolomitization and moldic porosity formation; stage 2, early oil charge; stage 3, TSR dissolution and cementation, gas charge, and bitumen formation; stage 4, post-TSR calcite cementation and dissolution, see text for details of each stage.

Table captions

Table 1. Point counting data showing percentages of each component in lime-grainstone and dolo-grainstone reservoirs in the Feixiangian Formation.

Table 2. $\delta^{13}C$‰, $\delta^{18}O$‰, and $^{87}Sr/^{86}Sr$ values of various types of carbonate minerals in lime-grainstone and dolo-grainstone reservoirs in the Feixianguan Formation.

Table 3. Four types of carbonate reservoirs classified on the basis of sedimentary facies in the Feixianguan Formation. Data are modified from an internal company report from Sinopec.

Figure 1. A) Paleogeography and locations of the sampled gas fields. The Feixianguan Formation dolomite reservoirs in the NE Sichuan Basin. B) Cross section (from A to B in part A) showing stratigraphic relationships and sedimentary facies distribution of the Feixianguan and Changxing formations. Modified from Jiang et al. (2014b).

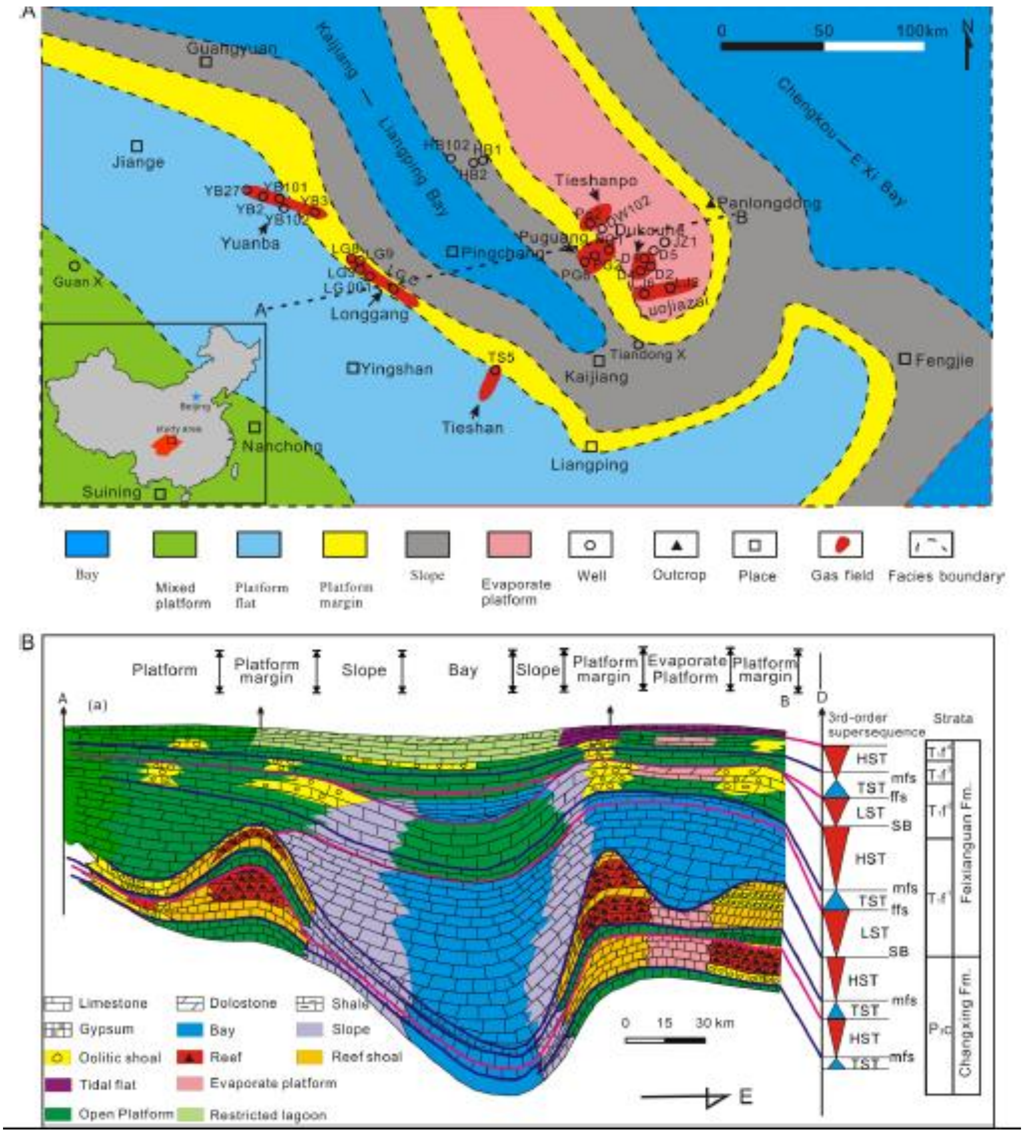

Figure 2. A) Stratigraphic and porosity correlation of the oolitic limestone and dolostone in the Feixianguan Formation across the open platform on the southwest side of Kaijiang–Liangping Bay to the restricted platform on the northwest side in Sichuan Basin (Fig. 1B). B) Core samples from well LG-001 showing the contrast reservoir quality between the dolostone section and limestone section: dolostone is porous and shows good moldic porosity whereas limestone is tight and enriched in stylolites and calcite cement. C) Core-derived porosity-permeability data of oolitic limestone reservoir in the Yuanba gas field, data modified from Cai et al. (2014). D) Core-derived porosity-permeability data of ooids enriched dolostone reservoir in the Puguang 2 well, data modified from Ma et al. (2008b).

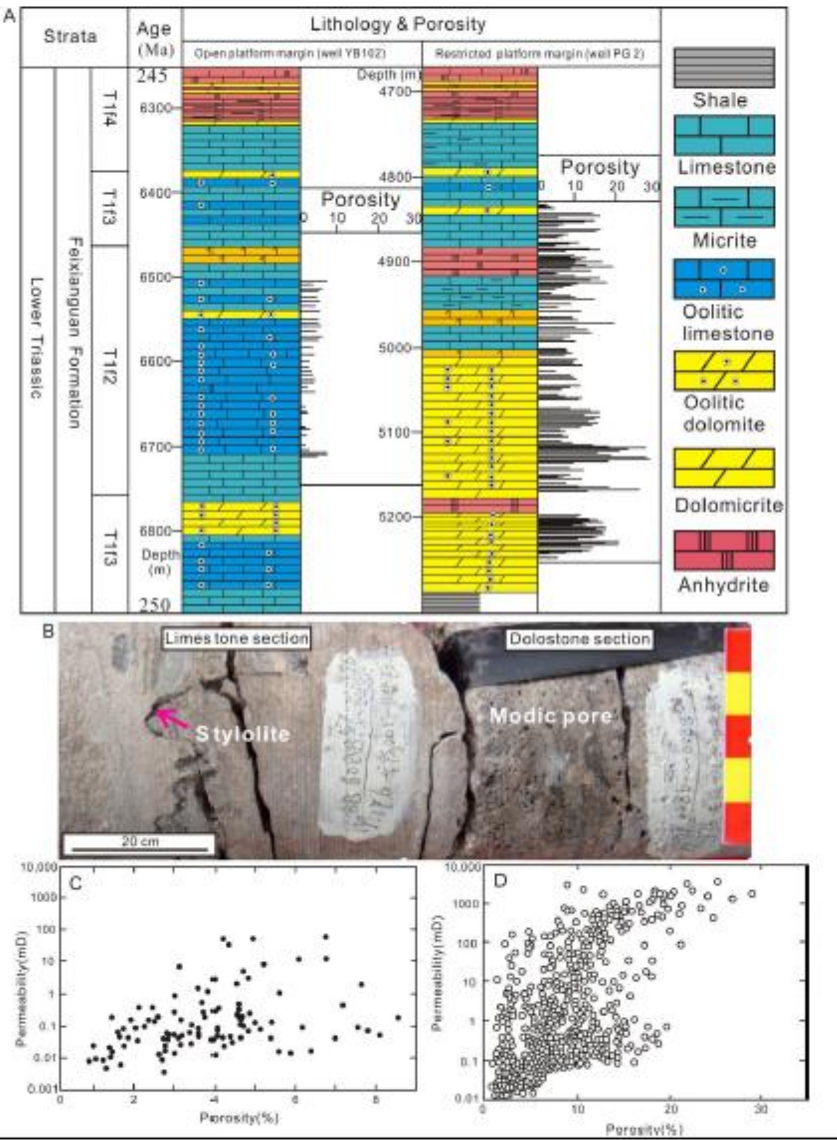

Figure 3. Burial and paleo-temperature histories constructed of well PG2 (A) and (B) well YB2 from the East Sichuan Basin, modified from Cai et al. (2014). Isotherms were constrained by vitrinite reflectance and fluid inclusion measurements.

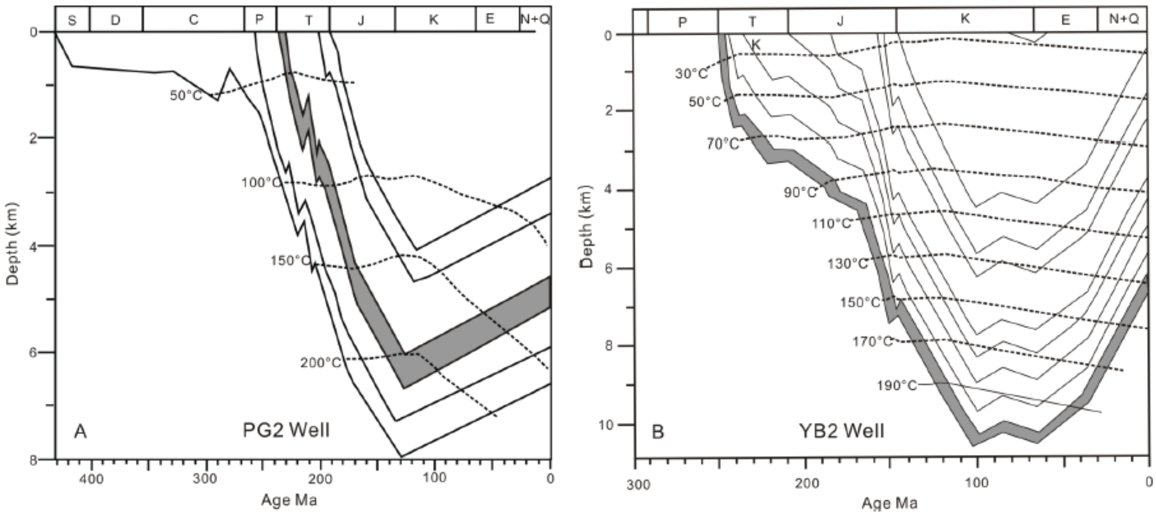

Figure 4. Different types of calcite cements and stylolite from the limestone in the Feixianguan Formation, well LG001, depth 6088.8 m. A) Calcite-1 and calcite-2 in limestone, open oomodic pores (red epoxy; yellow arrow) locally present, well HB2, 5,104.3m. B) Calcite-2 (in red) filling in moldic porosity and interparticle pores in limestone, well YB2, depth 6428 m. C) Photomicrograph shows tight limestone with minimal visual porosity due to the presence of stylolite (red arrow) and volumetrically-important calcite-3 cementation.

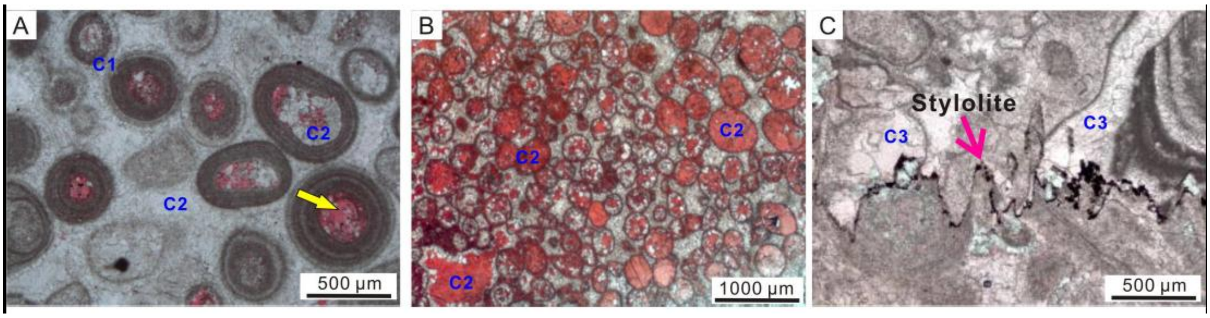

Figure 5. Different types of calcite cements precipitated in various diagenetic environments in dolostone in the Feixianguan Formation (A, B, C are photomicrograph figures, D is a photo of BSEM). A) Calcite-3 (red) filling in fracture in dolomite reservoir, well LJ1, 3,470.40 m. B) Oil-stage TSR calcite-4 (red) and bitumen (black) filling in dissolution-enlarged pores (blue proxy) in dolomite reservoir, dissolution pores locally present in calcite-3, micrite envelopes (yellow arrow) developed in the edges of ooids, well LJ2, 3,232.9m. C) Gas-stage TSR calcite-4 (red) does not contain bitumen or oil inclusions filling (black) in dissolution pores in dolomite reservoir, well LJ6, 3,936.00 m. D) Late stage post-TSR calcite-5 (light gray) filling in fractures in the dolomite reservoir, well DW102, depth 4901 m.

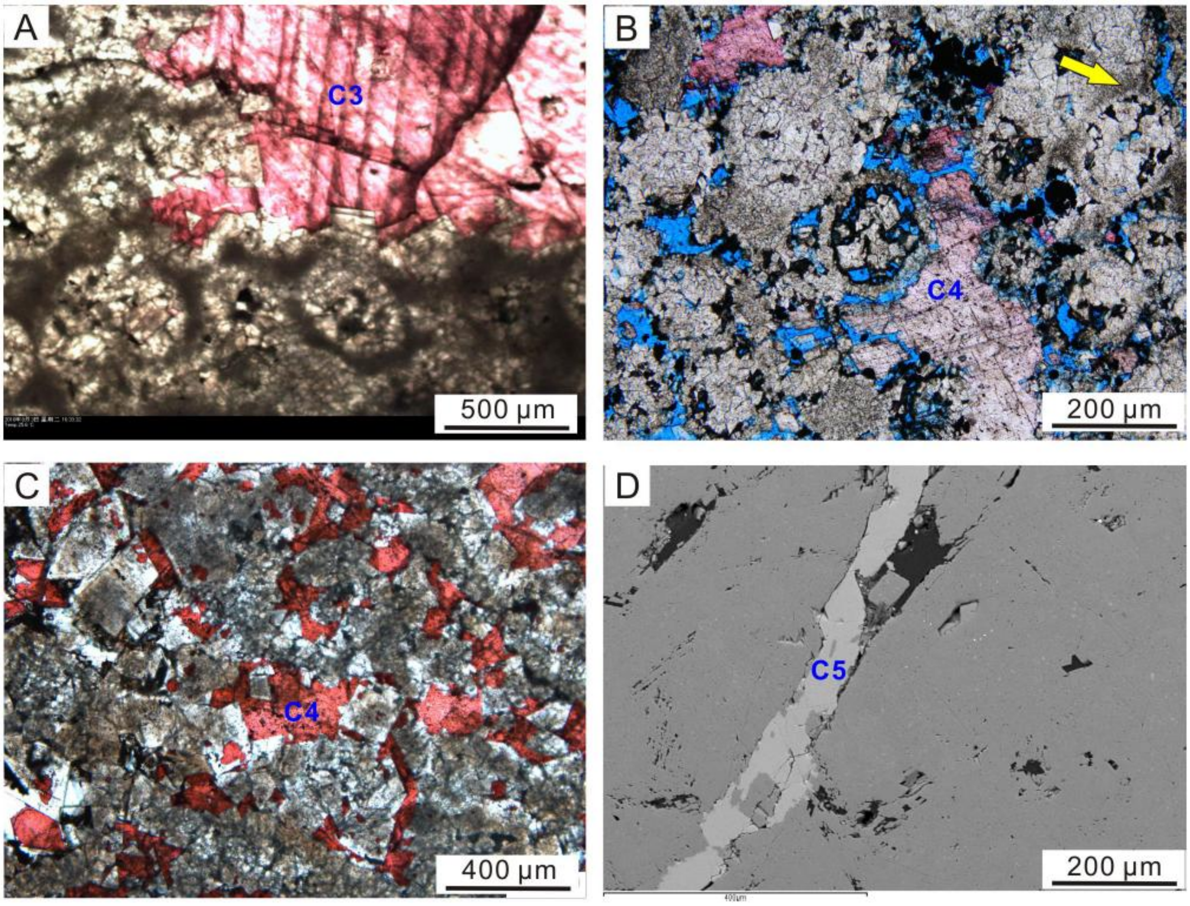

Figure 6. Photomicrographs showing different preservation of original ooid textures in dolomite reservoirs. A) Micro-crystalline dolomite with early replaced dolomite cement (red arrow), the original ooid texture is well persevered, white space stand for pore space, well PG2, 4977.4 m; B) Coarsely crystalline, fabric destructive dolomite, the original ooid texture cannot be discerned due to severe recrystallization, abundant intercrystalline porosity (blue) is present, well LJ2, 3,232.2 m.

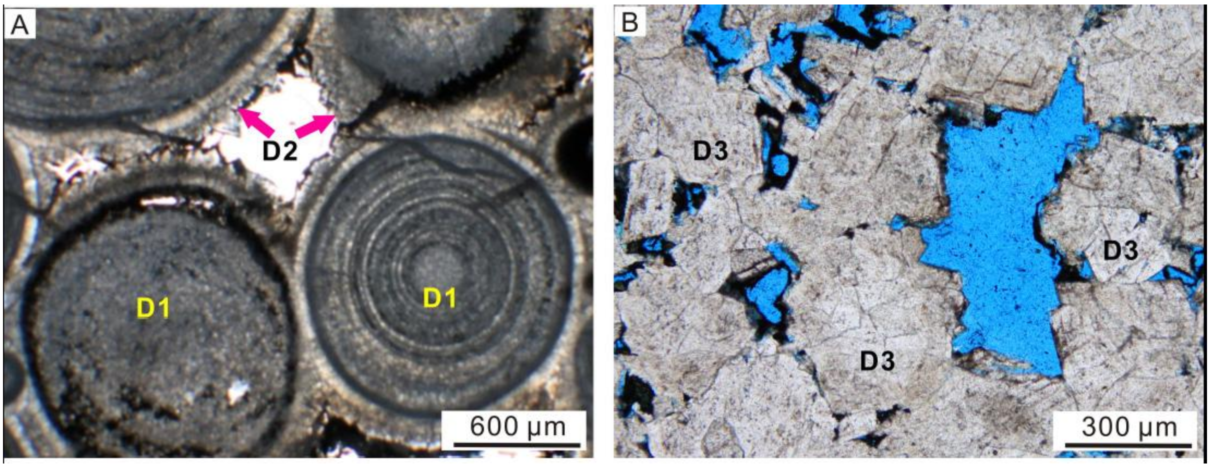

Figure 7. Photomicrographs show different types of dissolution porosity in dolomite reservoirs. A) Partially dissolved moldic porosity (red) developed in ooids, well PG2, depth 5130 m. B: Open mold (red) show completely dissolution of the ooids, well PG2, depth 5133 m. C) Dissolution enlarged porosity up to millimetres range (blue) with some ooids completely dissolved, LJ2 3,232.9 m. D) Late dissolution of coarse dolomite crystals, which were partially or completely dissolved (red), locally filling with bitumen, well PG2, depth 5130 m.

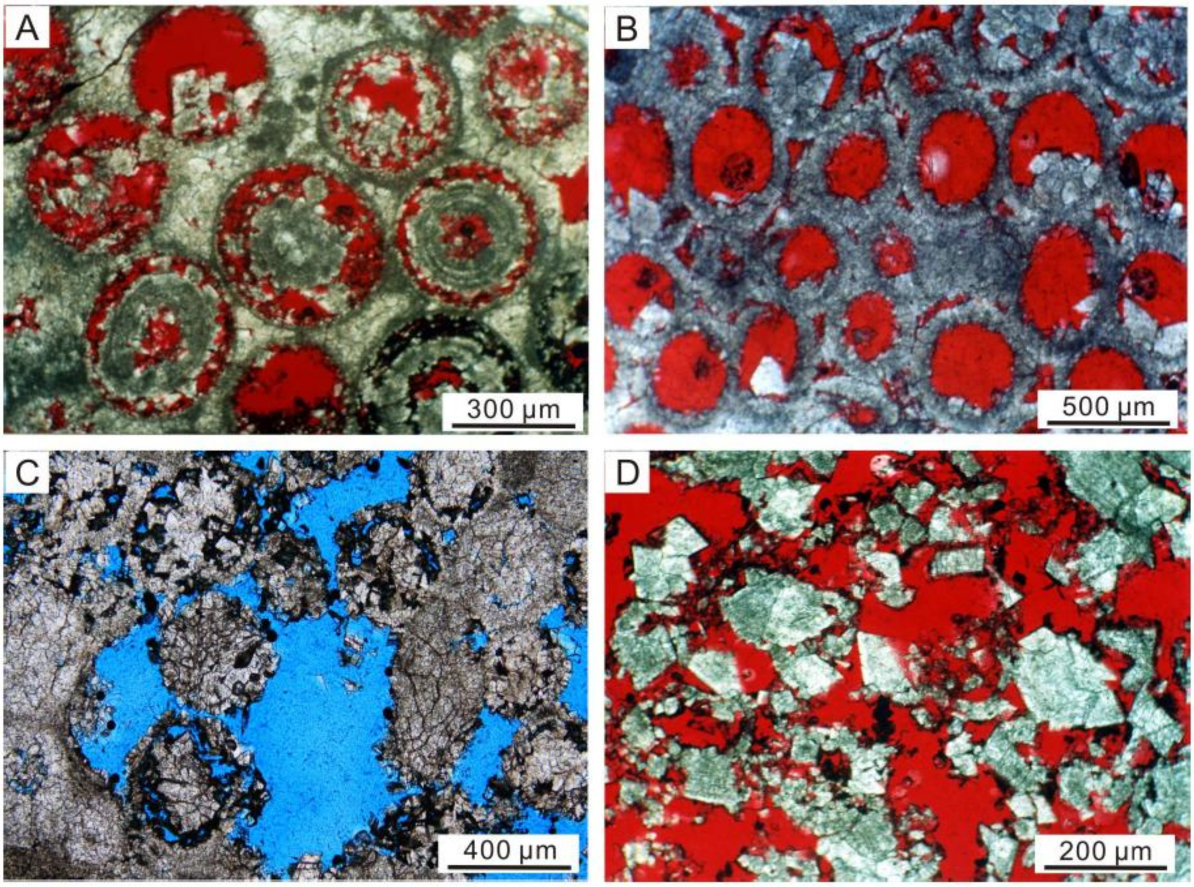

Figure 8: Photomicrographs (A, B) and BSEM images (C, D) show other non-carbonate minerals in dolomite reservoirs. A) Early anhydrite cement (marked as A) filling in both interparticle and intraparticle porosities of dolostone (marked as D), well PG11, 5,818.00 m. B) Late stage quartz cement (marked as Q) filling in dissolution enlarged pores in dolostone (marked as D), well D2, depth 4300 m. C) Pyrite (marked as Py) filling in dissolution pores in dolostone (marked as D), D2-25, depth 4309 m. D) Barite (marked as Ba) associated with fluorite (marked as F) and calcite (marked as C) filling in a fracture, well P2-30.

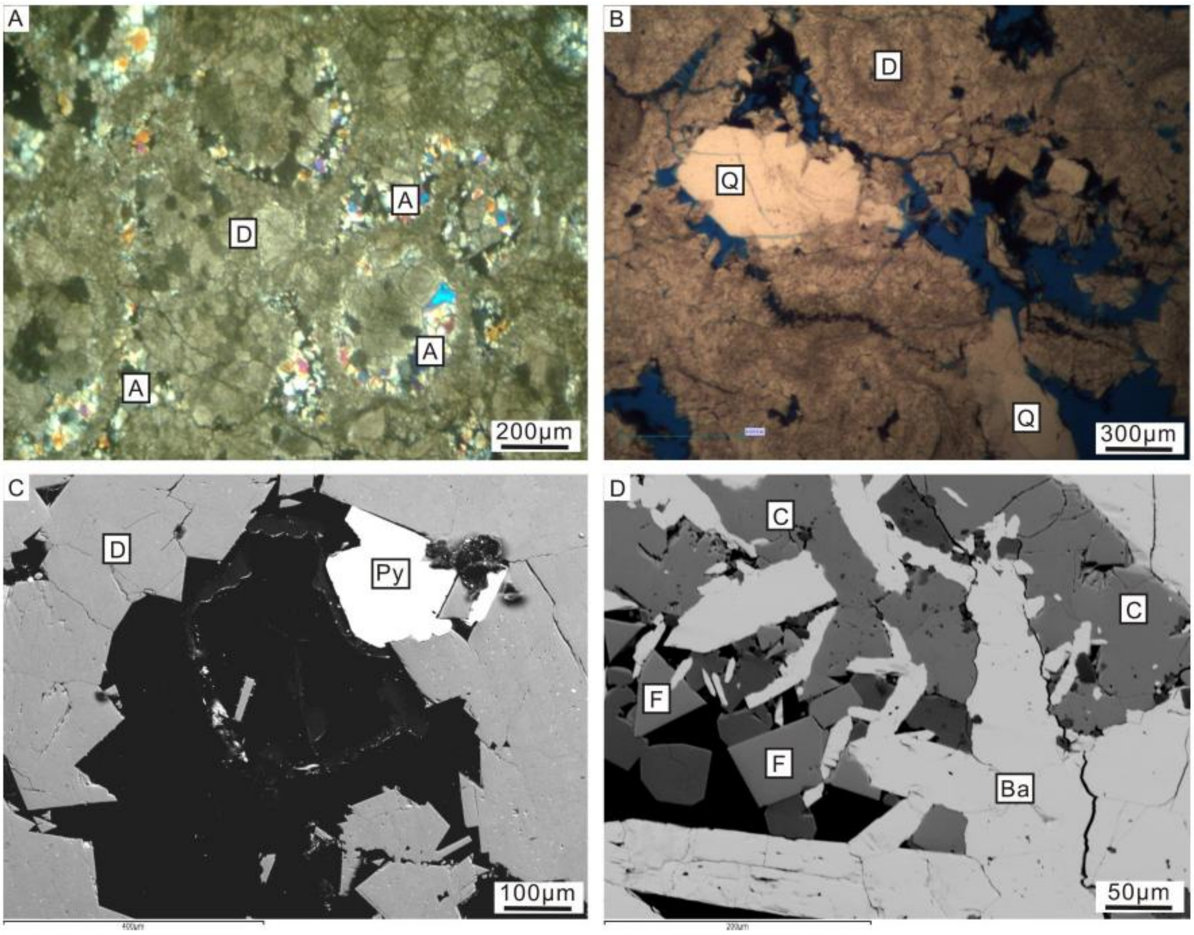

Figure 9: Photomicrographs show three generation of fractures in dolomite reservoir. A) Fracture-1 crosscut by fracture-2, both of which were filled with calcite-3 cement, well HB2-5, depth 5105.2 m. B) Fracture-3 cross-cutting all the other minerals suggesting that it represents the latest fracture stage, and it locally remains open (red) without any mineral in-filling, well PG2, depth 5103 m.

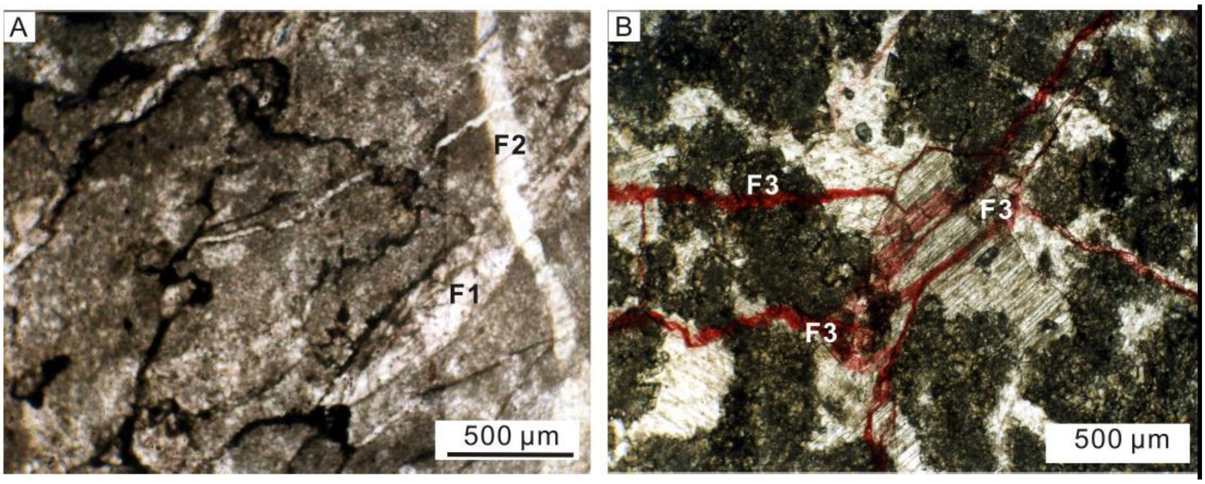

Figure 10: Compositions of oolitic limestone (A) and oolitic dolomite (B). Original porosity in limestone was nearly completely filled by early calcite, thus limestones show negligible late diagenetic minerals or dissolution porosity. In contrast, dolostone reservoirs contain only minor quantities of early calcite cement and have much higher remaining porosity and quantities of late diagenetic minerals dominated by dolomite and bitumen.

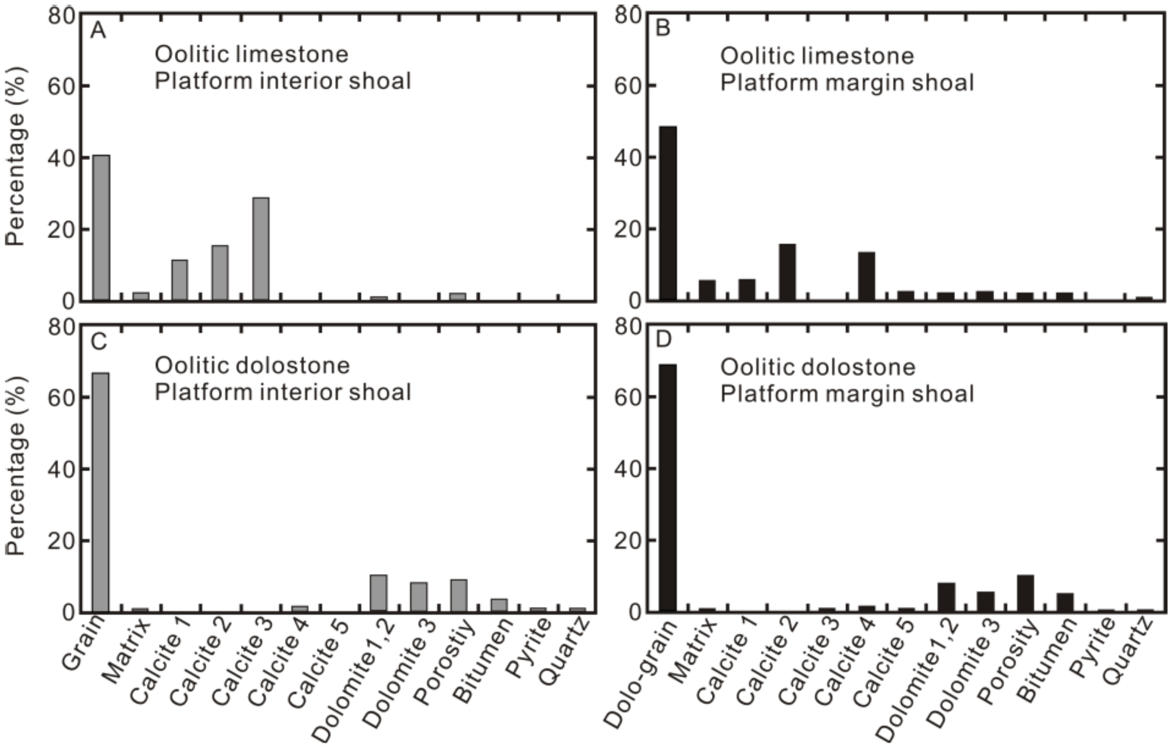

Figure 11: Fluid-inclusion data obtained from different types of calcite in the Feixianguan Formation. A) Fluid-inclusion homogenization temperatures from aqueous inclusions from pre-TSR calcite (calcite-2). B) Salinity of aqueous inclusions from calcite-2. C) Fluid-inclusion homogenization temperatures from two-phase aqueous inclusions from TSR calcite-4 (those with oil or bitumen inclusions are oil stage TSR calcite; those without are gas stage TSR calcite). D) Salinity of aqueous inclusions from TSR calcite-4. E) Fluid-inclusion homogenization temperatures from two-phase aqueous inclusions from post-TSR calcite (calcite-5). F) Salinity of aqueous inclusions from calcite-5. Fluid inclusion data from dolostone reservoirs are adapted from Jiang et al. (2015a).

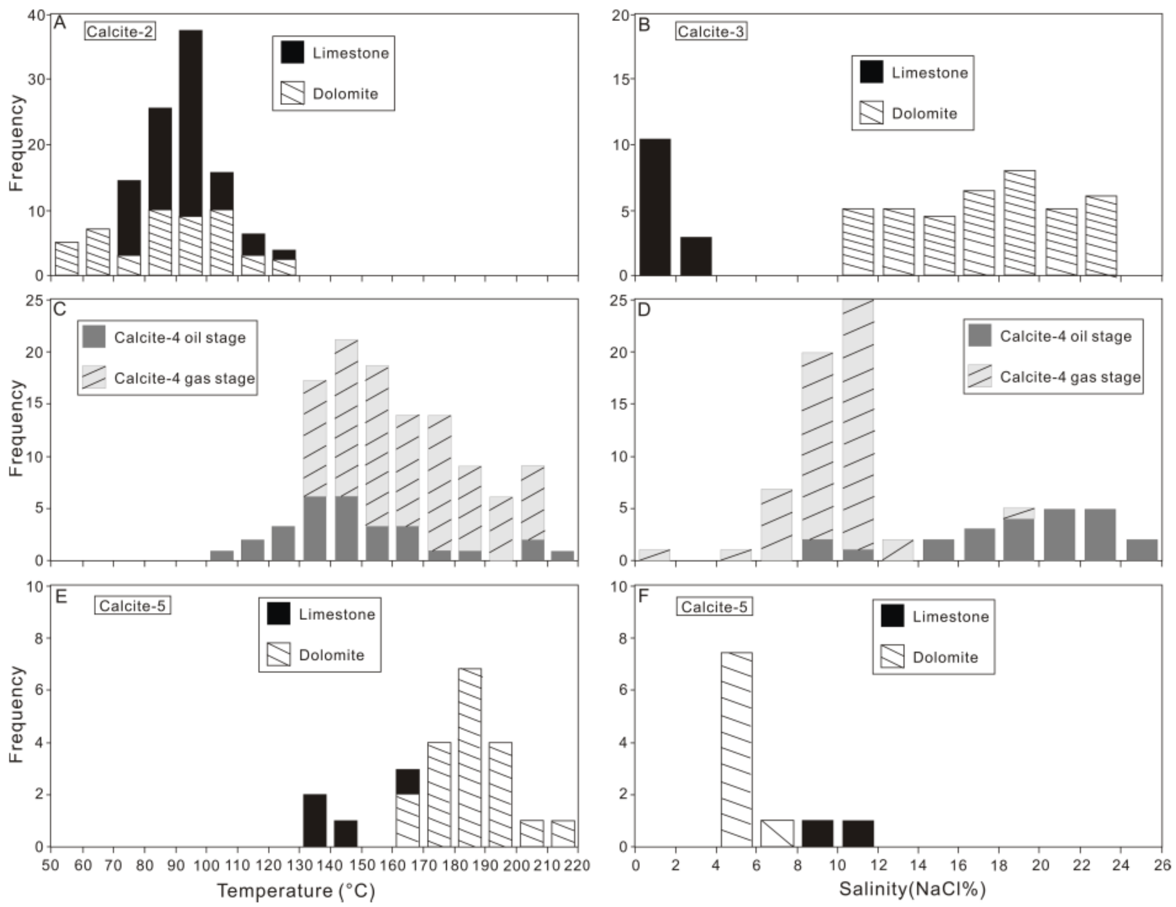

Figure 12: A) Average salinity and homogenization temperature data from fluid inclusions in calcite cements in limestone. B) Average salinity and homogenization temperature from fluid inclusions in pre-TSR, TSR, and post-TSR calcite in dolomite, adapted data from Jiang et al. (2015c).

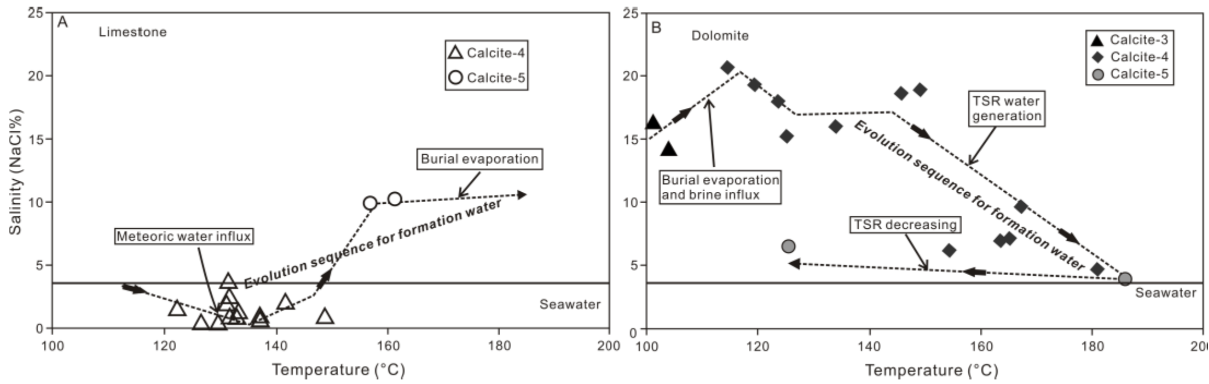

Figure 13: Carbon and oxygen isotopic compositions of (A) limestone and (B) dolostone from the Feixianguan Formation in the NE Sichuan Basin. Dash open rectangles are adapted from previous studies (Jiang et al., 2014a; Jiang et al., 2015a; Jiang et al., 2015c); red rectangle filled with red symbols is from this study.

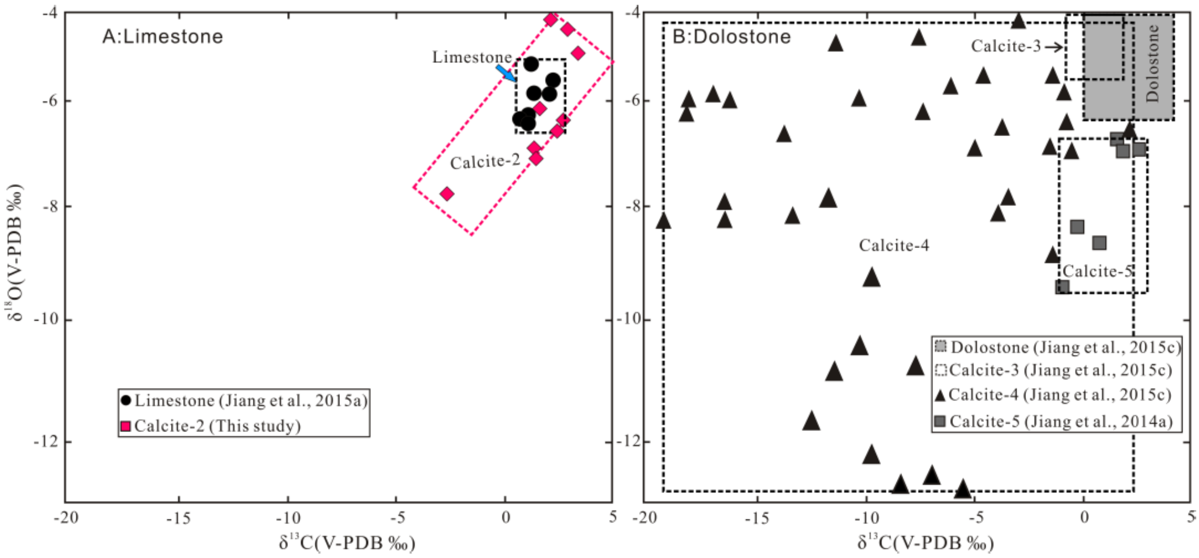

Figure 14: $^{87}Sr/^{86}Sr$ ratios of various types of carbonate minerals in (A) limestone and (B) dolostone, in comparison with those from literature data for coeval seawater from the Lower Triassic Feixianguan Formation in NE Sichuan Basin, China. Sr isotope and age data for the Feixianguan and Jialingjiang seawater from Jiang et al. (2014b).

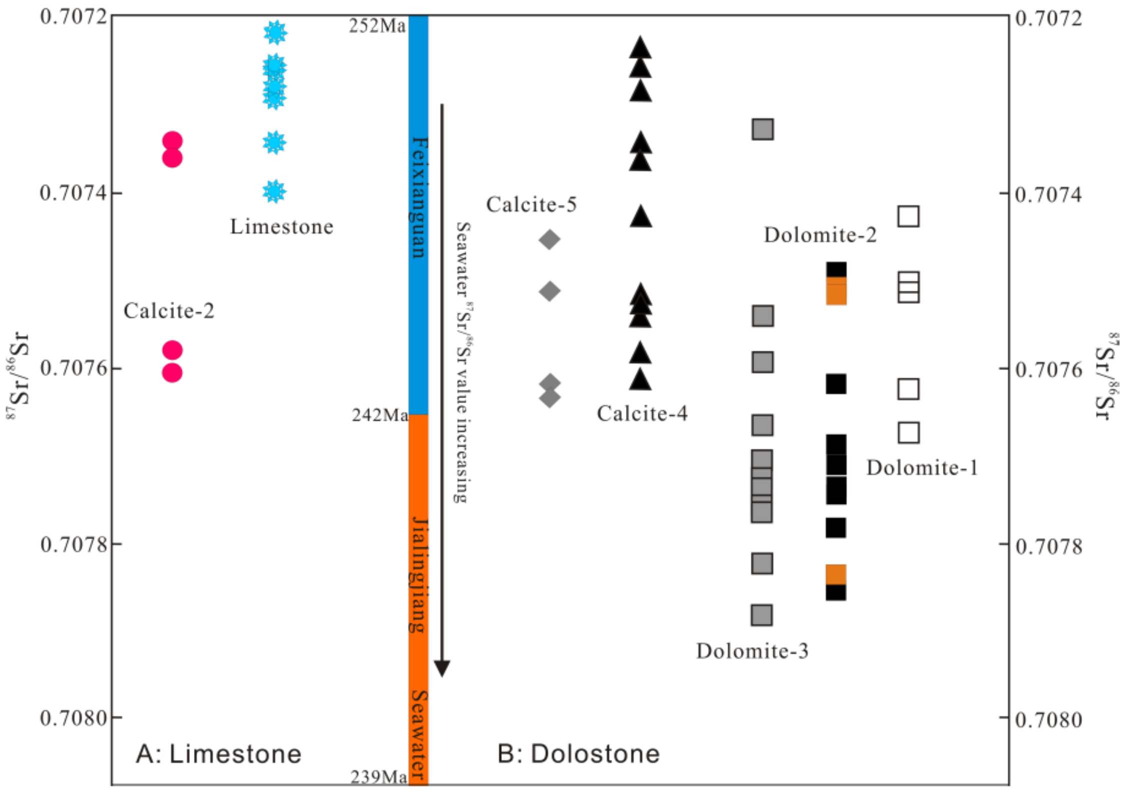

Figure 15. Paragenetic sequence of A) limestone and B) dolostone in the Feixianguan Formation in northeast Sichuan Basin, summarizing major products of pre-TSR diagenesis, TSR diagenesis, post-TSR diagenesis, and the temperature for each diagenetic realms. Temperature data are from fluid inclusion analysis. Time scale bar was added by combing the burial histories in Figure 3 with fluid inclusion data.

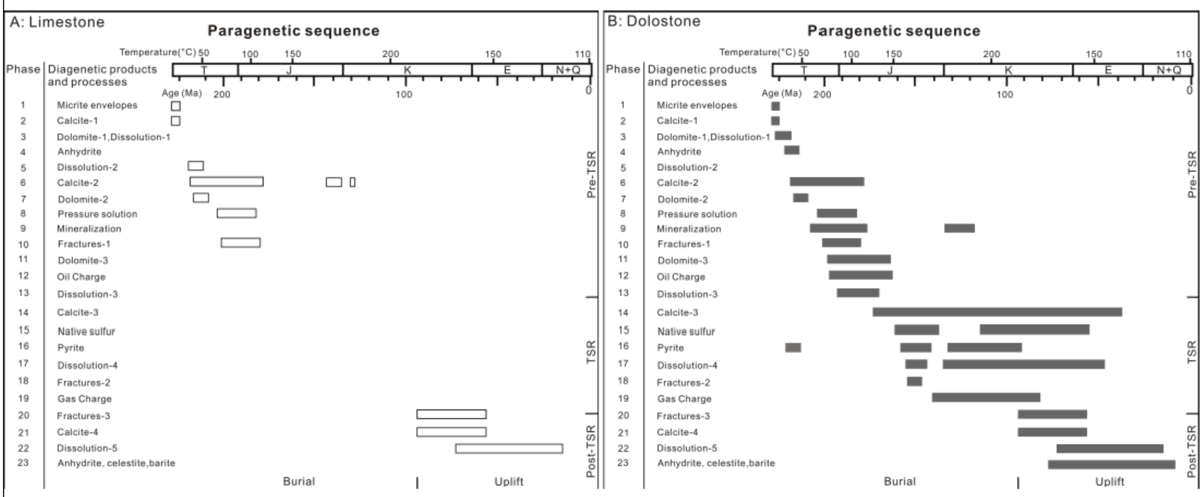

Figure 16: Limestone reservoir evolution models for the Feixianguan Formation. The model has been divided into three different diagenetic stages, which are here considered to be important for reservoir quality evolution. Each stage has distinguishable diagenetic fluids, products, and porosity. They are: stage 1, meteoric water dissolution and cementation; stage 2, mechanical compaction, pressure solution, and calcite cementation; stage 3, post-TSR calcite cementation, see text for details of each stage. Porosity in each diagenetic stage was calculated by the average point count data of lime-grainstone and dolo-grainstone in Table 1.

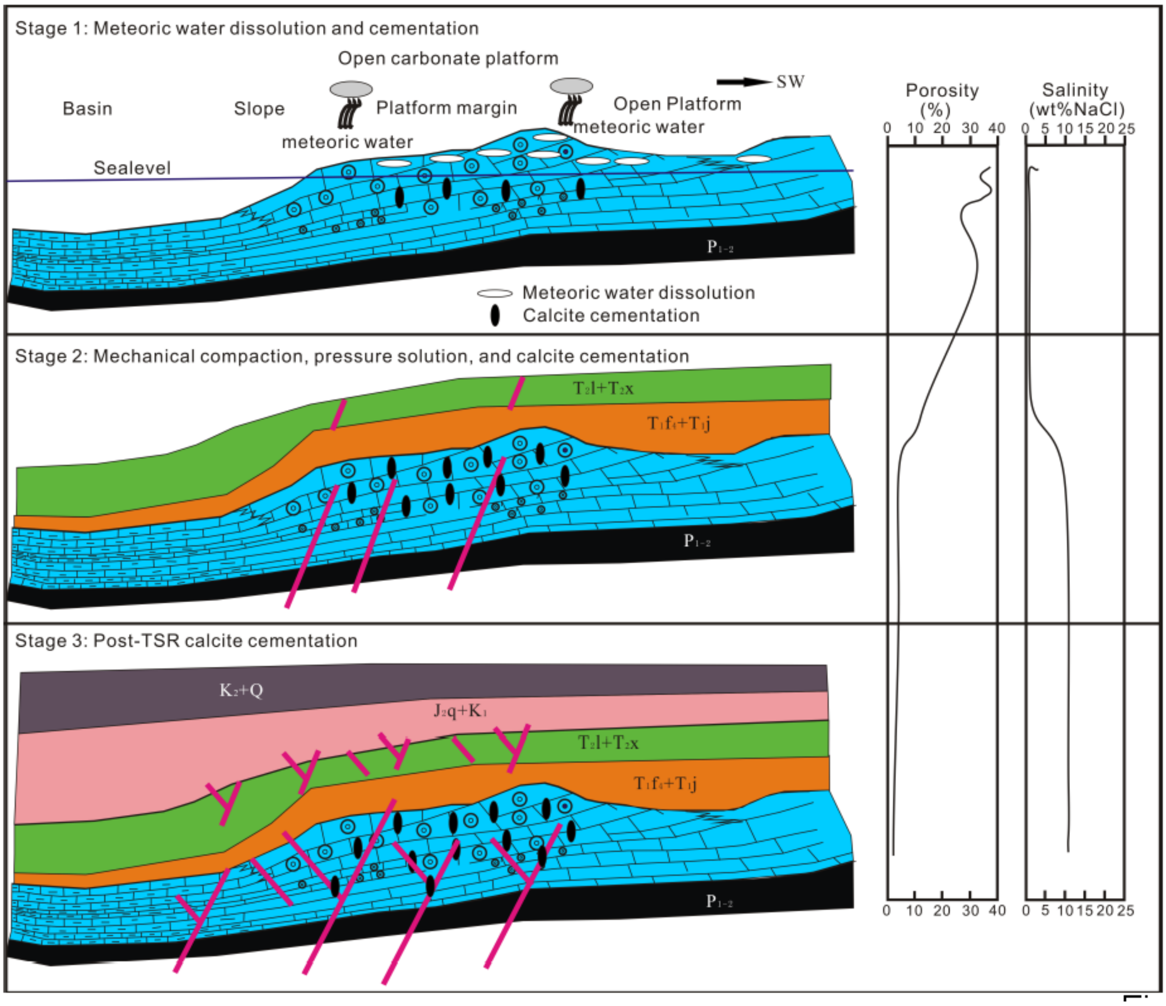

Figure 17: Dolostone reservoir evolution models for the Feixianguan Formation. The models have been divided into four different diagenetic stages, which are here considered to be important for reservoir quality evolution. Each stage has distinguishable diagenetic fluids, products, and porosity. They are: stage 1, early dolomitization and moldic porosity formation; stage 2, early oil charge; stage 3, TSR dissolution and cementation, gas charge, and bitumen formation; stage 4, post-TSR calcite cementation and dissolution, see text for details of each stage.

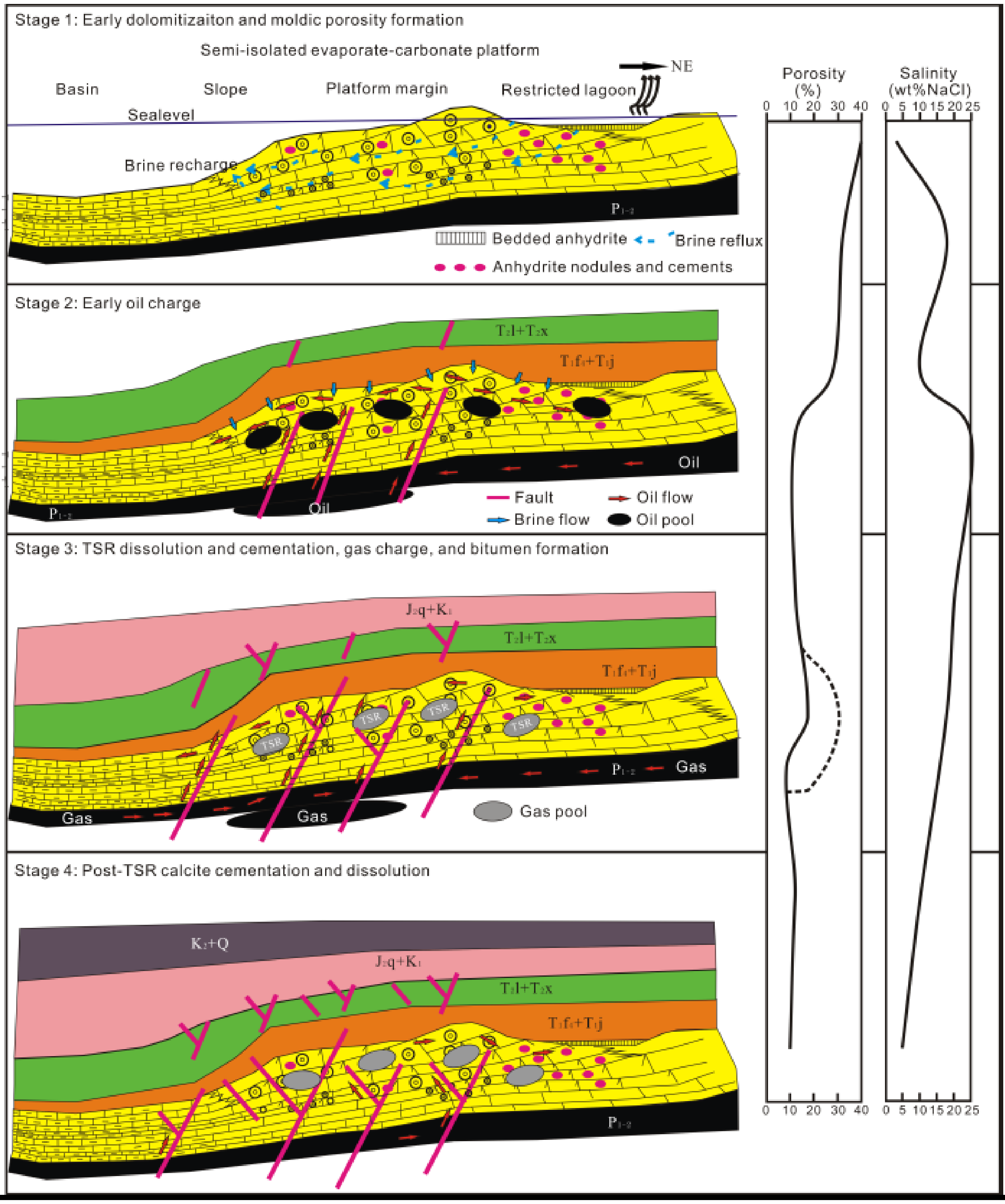

Table 1. Point counting data showing percentages of each component in lime-grainstone and dolo-grainstone reservoirs in the Feixiangian Formation

Sample No.	Depth (m)	Location	Facies (Shoal)	Rock type	Grain (%)	Matrix (%)	Carbonate cement (%) C1	C2	C3	C4	C5	D1,2	D3	Porosity (%)	Bitumen (%)	Pyrite (%)	Quartz (%)
HB1-5a	4972	NE Side	Interior	O L	26	0	16	27	25	0	0	0	0	6	0	0	0
HB1-5b	4972	NE Side	Interior	O L	26	0	41	0	19	0	0	7	0	7	0	0	0
HB1-5c	4973	NE Side	Interior	O L	56	0	2	24	16	0	0	0	0	2	0	0	0
HB1-5d	4973	NE Side	Interior	O L	48	0	0	23	29	0	0	0	0	0	0	0	0
HB1-5f	4974	NE Side	Interior	O L	35	3	7	20	28	0	0	2	0	5	0	0	0
HB2-5a	5104	NE Side	Interior	O L	42	0	5	10	41	0	0	0	0	2	0	0	0
HB2-5b	5106	NE Side	Interior	O L	45	0	6	3	45	0	0	0	0	1	0	0	0
HB2-5c	5017	NE Side	Interior	O L	46	0	10	9	31	0	0	0	0	4	0	0	0
HB2-5d	5112	NE Side	Interior	O L	55	0	18	10	15	0	0	2	0	0	0	0	0
HB102-4a	5174	NE Side	Interior	O L	55	0	5	10	30	0	0	0	0	0	0	0	0
HB102-4b	5177	NE Side	Interior	O L	46	0	24	11	16	0	0	3	0	0	0	0	0
J5	outcrop	SW Side	Interior	O L	29	0	10	40	20	0	0	0	0	0	1	0	0
J7	outcrop	SW Side	Interior	O L	43	0	7	17	33	0	0	0	0	0	0	0	0
J8	outcrop	SW Side	Interior	O L	11	26	5	10	48	0	0	0	0	0	0	0	0
DW102	outcrop	SW Side	Margin	O L	70	6	3	3	0	0	0	8	0	3	3	0	4
PLD-1	outcrop	SW Side	Margin	O L	60	0	4	6	0	0	20	0	0	10	0	0	0
PLD-2	outcrop	SW Side	Margin	O L	45	22	3	5	0	0	13	0	0	7	0	0	5
YB2-3	6401	SW Side	Margin	O L	45	0	3	5	40	0	0	0	5	0	2	0	0
YB2-4	6428	SW Side	Margin	O L	55	0	6	14	18	0	0	0	7	0	0	0	0
YB3-1a	6581	SW Side	Margin	O L	50	6	6	15	8	0	0	0	15	0	0	0	0
YB3-1b	6583	SW Side	Margin	O L	36	25	6	15	10	0	0	0	8	0	0	0	0
YB3-2	6627	SW Side	Margin	O L	23	18	10	20	28	0	0	1	0	0	0	0	0
YB101-2	6797	SW Side	Margin	O L	54	0	5	6	30	0	0	1	2	0	0	0	2
YB102-4a	6597	SW Side	Margin	O L	34	0	10	29	0	0	0	17	0	1	9	0	0
YB102-4b	6600	SW Side	Margin	O L	27	0	8	53	0	0	1	4	0	0	7	0	0
YB102-5a	6602	SW Side	Margin	O L	44	0	7	24	18	0	0	0	0	2	3	0	2
YB102-5b	6605	SW Side	Margin	O L	65	1	6	6	13	0	0	0	0	8	1	0	0
LGC	5935	SW Side	Margin	O L	63	0	5	12	20	0	0	0	0	0	0	0	0
LJ2-1	3198	NE Side	Interior	OD	67	6	0	0	0	0	2	7	2	6	9	0	1
LJ2-18	3267	NE Side	Interior	O D	70	0	0	0	0	0	0	15	8	5	2	0	0
LJ2-25	3256	NE Side	Interior	O D	65	0	0	0	0	0	0	15	5	8	5	2	0
LJ2-33	3232	NE Side	Interior	O D	75	0	0	0	0	0	0	0	15	8	2	0	0
LJ2-37	3233	NE Side	Interior	O D	56	0	0	0	0	4	0	17	0	20	3	0	0
LJ2-26	3256	NE Side	Interior	O D	71	0	0	0	0	0	0	0	17	8	1	3	0
LJ3-58	--	NE Side	Interior	O D	69	0	0	0	0	2	0	10	5	13	0	1	0
LJ3-27	--	NE Side	Interior	O D	66	0	0	0	0	0	0	18	7	3	6	0	0
LJ2	--	NE Side	Interior	O D	71	0	0	0	0	2	0	8	15	2	1	1	0
LJ2-23	--	NE Side	Interior	O D	67	0	0	0	0	0	0	25	0	3	5	0	0
D1	--	NE Side	Margin	O D	58	0	0	0	0	3	0	17	4	9	8	0	1
D2-25	4309	NE Side	Margin	O D	62	0	0	0	0	5	0	0	20	10	1	2	0
D2-7	--	NE Side	Margin	O D	57	0	0	0	0	0	0	0	18	16	2	2	5
D4-4	4236	NE Side	Margin	O D	78	0	0	0	0	4	0	5	0	13	0	0	0
D5	4793	NE Side	Margin	O D	55	0	0	0	0	3	0	11	6	12	9	0	4
DW102	4901	NE Side	Margin	O D	71	9	0	0	17	3	0	0	0	0	0	0	0
PLD-3	outcrop	NE Side	Margin	O D	80	0	0	0	0	0	6	0	0	0	12	2	0
PLD-4	outcrop	NE Side	Margin	O D	72	0	0	0	0	0	14	0	0	0	14	0	0
LJ6-7	3936	NE Side	Margin	O D	65	0	0	0	0	0	0	12	8	8	7	0	0
PG1a	--	NE Side	Margin	O D	70	0	0	0	0	0	0	12	0	17	1	0	0
PG1b	--	NE Side	Margin	O D	72	0	0	0	0	0	0	5	5	17	1	0	0
PG2-24	5020	NE Side	Margin	O D	63	0	0	0	0	0	0	10	0	27	0	0	0
PG2-21	4987	NE Side	Margin	O D	60	0	0	0	0	0	0	0	14	25	1	0	0
PG2-20a	4978	NE Side	Margin	O D	83	0	0	0	0	0	0	12	0	3	2	0	0
PG2-27	5043	NE Side	Margin	O D	75	0	0	0	0	0	0	18	0	5	2	0	0
PG2-31	5076	NE Side	Margin	O D	72	0	0	0	0	0	0	5	20	0	3	0	0
PG2-32	5085	NE Side	Margin	O D	74	0	0	0	0	0	0	7	14	3	2	0	0
PG2-41	5196	NE Side	Margin	O D	70	0	0	0	0	0	0	13	5	10	2	0	0
PG2-39	5166	NE Side	Margin	O D	65	0	0	0	0	0	0	10	8	17	0	0	0
PG2-22a	4980	NE Side	Margin	O D	64	0	0	0	0	0	0	0	20	14	2	0	0
PG2-26	4937	NE Side	Margin	O D	75	0	0	0	0	0	0	13	0	12	0	0	0
PG2-21	4934	NE Side	Margin	O D	80	0	0	0	0	6	0	0	7	7	0	0	0
PG2-22b	4935	NE Side	Margin	O D	64	0	0	0	0	17	0	0	15	0	4	0	0
PG2-5	4776	NE Side	Margin	O D	67	0	0	0	0	14	0	0	5	13	0	0	1
PG2-20b	4982	NE Side	Margin	O D	38	0	0	0	0	0	0	12	17	33	0	0	0
PG2-30	5066	NE Side	Margin	O D	87	0	0	0	0	0	0	0	0	12	1	0	0
PG6-a	--	NE Side	Margin	O D	60	0	0	0	0	0	0	18	7	10	5	0	0
PG6-b	--	NE Side	Margin	O D	68	0	0	0	0	0	0	0	0	2	26	4	0
PG6-c	5142	NE Side	Margin	O D	75	0	0	0	0	0	0	0	18	5	2	0	0
TS 5-9	--	SW Side	Margin	O D	66	0	0	0	0	3	0	14	0	6	11	0	0
TS 5-11	--	SW Side	Margin	O D	56	0	0	0	0	0	0	14	0	18	12	0	0
TS 5-12	--	SW Side	Margin	O D	49	0	0	0	0	1	0	24	0	10	16	0	0
TS 5-13	--	SW Side	Margin	O D	53	18	0	0	0	2	0	14	0	2	11	0	0
LGC	5933	SW Side	Margin	O D	65	0	0	0	0	3	0	17	0	13	2	0	0
Average value			Lime-grainstone		44.1	3.8	8.5	15.3	20.8	0	1.2	1.6	1.3	2.1	0.9	0.0	0.5
			Dolo-grainstone		67.0	0.8	0.0	0	0.4	1.6	0.5	8.6	6.5	9.7	4.4	0.4	0.3

NE Side: Northeast side of the Kaijiang-Liangping Bay; SW Side: Southwest side of the Kaijiang-Liangping Bay; OL: oolitic limestone; OD: oolitic dolostone

Table 2. $\delta^{13}C$‰, $\delta^{18}O$‰, and $^{87}Sr/^{86}Sr$ values of various types of carbonate minerals in lime-grainstone and dolo-grainstone reservoirs in the Feixianguan formation

Sample	Depth (m)	Location	Lithology	Mineral	$\delta^{13}C$‰	$\delta^{18}O$‰	$^{87}Sr/^{86}Sr$
LG3	5935.9	SW Side	Limestone	Micrite	--	--	0.707280
LG3	--	SW Side	Limestone	Micrite	--	--	0.707130
LG8	6523.4	SW Side	Limestone	Micrite	--	--	0.707399
LG8	6526.0	SW Side	Limestone	Micrite	--	--	0.707344
LG8	6524.1	SW Side	Limestone	Micrite	--	--	0.707130
LG8	6526.1	SW Side	Limestone	Micrite	--	--	0.707345
LG8	6527.8	SW Side	Limestone	Micrite	--	--	0.707220
TS5	--	SW Side	Limestone	Micrite	--	--	0.707460
LG001	6141.5	SW Side	Dolostone	Dolomite-2	--l	--	0.707508
LG001	6142.6	SW Side	Dolostone	Dolomite-2	--	--	0.707823
LG001	5990.1	SW Side	Dolostone	Dolomite-2	--	--	0.707518
YB101	--	SW Side	Dolostone	Calcite-2	3.44	-4.41	--
YB205	--	SW Side	Dolostone	Calcite-2	2.79	-5.72	--
YB27	--	SW Side	Dolostone	Calcite-2	2.46	-5.93	--
YB271	--	SW Side	Dolostone	Calcite-2	2.95	-3.99	--
EL-1	outcrop	SW Side	Dolostone	Calcite-2	2.19	-3.78	--
EL-3	outcrop	SW Side	Dolostone	Calcite-2	-2.53	-7.17	--
EL-16	outcrop	SW Side	Dolostone	Calcite-2	-0.11	-3.95	--
TS5-11	--	SW Side	Dolostone	Calcite-3	--	--	0.707581
TS5-13	--	SW Side	Dolostone	Calcite-3	--	--	0.707607
LG3	5935.5	SW Side	Dolostone	Calcite-3	1.53	-6.45	0.707344
LG8	6523.3	SW Side	Dolostone	Calcite-3	1.44	-6.30	0.707363
LG9	5870.1	SW Side	Dolostone	Calcite-3	1.66	-5.51	--

-- Not measured or no data available; SW Side: Southwest side of the Kaijiang-Liangping Bay

Table 3. Four types of carbonate reservoirs classified on the basis of sedimentary facies in the Feixianguan Formation. Data are modified from a report from Sinopec.

Sedimentary Facies	Porosity (%)			Permeability (mD)		
	Number	Range	Average	Number	Range	Average
Slope	21	0.9-1.8	1.4	21	0.01-0.43	0.06
Restricted platform	84	1.3-20.9	3.1	57	0.00-41.54	1.49
Platform margin Shoal	744	1.11-28.9	9.24	664	0.02-7973.77	174.81
Evaporative platform	591	0.45-17.2	4.5	526	0.00-9664.89	81.94